Pergamon

0148-9062(93)E0023-H

Int. J. Rock Mech. Min. Sci. & Geomech. Abstr. Vol. 31, No. 4, pp. 293–312, 1994

0148-9062/94 $7.00 + 0.00

Gravitational Stresses in Long Symmetric Ridges and Valleys in Anisotropic Rock

ERNIAN PAN†
BERNARD AMADEI†
WILLIAM Z. SAVAGE‡

The effect of topography and rock mass anisotropy on gravitational stresses in long isolated symmetric ridges and valleys is modeled using an analytical method proposed earlier by the first two authors. The rock mass deforms under a condition of plane strain. A parametric study is presented on the effect of (1) topography, (2) orientation of anisotropy and (3) degree of anisotropy on the magnitude and distribution of gravitational stresses in transversely isotropic rock masses with planes of anisotropy striking parallel to the ridge or valley axis. It is found that compressive stresses develop near ridge crests and that tensile stresses develop in valley bottoms and valley walls. The magnitude of the gravitational stresses is of the order of the characteristic stress $\rho g|b|$ where ρ is the rock density, g is the gravitational acceleration and $|b|$ is the height of the ridge or depth of the valley.

INTRODUCTION

When estimating the state of stress at any depth, z, in a rock mass due to gravity, several assumptions are commonly made. First, the rock mass is an isotropic and linearly elastic continuum. Second, the ground surface is horizontal. Third, the state of stress is described by two components: a vertical component σ_v due to the weight of overlying rock at that depth and equal to γz, and a horizontal component σ_h equal to K times σ_v. Fourth, σ_h is assumed to be uniform in the horizontal plane. Finally, σ_v and σ_h are assumed to be principal stresses. In general, these simplifying assumptions break down when the ground surface is not horizontal or when the rock mass is anisotropic.

The effect of anisotropy on gravitational stresses in rock masses with a horizontal ground surface has been addressed by Amadei *et al.* [1, 2] and Amadei and Savage [3] for orthotropic and transversely isotropic rock masses with horizontal or vertical anisotropy under a condition of no lateral displacement. Both homogeneous and stratified rock masses were considered. Amadei and Pan [4] proposed closed-form solutions for gravitational stresses in anisotropic rock masses with inclined planes of anisotropy under a condition of no lateral horizontal strains. These analytical solutions show that the vertical and horizontal gravity-induced stresses are principal stresses with $\sigma_v = \gamma z$ and that the horizontal stress magnitude greatly depends on the type, degree, and orientation of rock anisotropy. More recently, the authors became aware of some early work done by Dolezalova [5] on gravitational stresses in cross-anisotropic soil deposits. She used a finite element analysis to show that for soil deposits with inclined layers and rigid lateral boundaries, the principal stresses are inclined with respect to the vertical and horizontal directions. The analyses of Dolezalova [5] and Amadei and Pan [4] illustrate the importance of boundary conditions on the type and magnitude of the gravitational *in situ* stress field.

The simplifying assumption that principal stresses are vertical and horizontal with depth breaks down when the ground surface is not horizontal. At the ground surface, principal stresses are parallel and perpendicular to the topography in the absence of surface loads. With depth, the principal stresses turn and approach the same directions as when the ground surface is horizontal. Knowing the effect of topography on stress distributions is of particular interest for the stability of underground excavations in mountainous regions near valley slopes. Phenomena such as rock bursts, spalling or fracturing may occur because of stress concentrations near valley walls [6, 7].

Analytically determining the stress distributions in a rock mass limited by a ground surface of complex topography by elastic theory is difficult. In the past, the effect of surface topography on gravitational stresses has

†University of Colorado, Department of Civil Engineering, Boulder, CO 80309-0428, U.S.A.
‡U.S. Geological Survey, Box 25046, MS 966, Denver, CO 80225, U.S.A.

been addressed by using two types of analytical methods. One is the exact conformal mapping method, as studied by Akhpatelov and Ter-Martirosyan [8], Ter-Martirosyan *et al.* [9], Ter-Martirosyan and Akhpatelov [10], Savage *et al.* [11] and Savage and Swolfs [12]. However, this approach is restricted to isotropic media, to a very few smooth topographic profiles for which conformal mapping functions can be found exactly, and to two-dimensional problems. The other approach for two- and three-dimensional problems in isotropic media is the perturbation method discussed by McTigue and Mei [13, 14] and Liu and Zoback [15]. Liao *et al.* [16] also used the perturbation method for two-dimensional problems in anisotropic media. The advantage of the perturbation method is that it can handle any smooth topographic feature. However, the solutions derived with that method are restricted to topographies with small slopes not exceeding 10%.

All the solutions derived with the exact conformal mapping and perturbation methods show clearly that the topography can have a major effect on the magnitude and distribution of stresses *in situ*. For instance, the expressions in Savage *et al.* [11] for gravitational stresses in long symmetric isotropic ridges and valleys clearly depend on the geometry of the topography as well as the rocks Poisson's ratio. It was found (1) that non-zero horizontal compressive stresses exceeding the vertical stress develop at and near ridge crests and (2) that horizontal tensile stresses develop under valleys. The horizontal compressive stresses in ridge crests decrease and the horizontal tensile stresses in valleys become more compressive with increasing Poisson's ratio. McTigue and Mei [13, 14] and Liao *et al.* [16] showed that topography affects gravitational stress distributions even in areas of low regional slopes. Liao *et al.* [16] also concluded that the magnitude of horizontal stresses in transversely isotropic and orthotropic ridges and valleys depends strongly on the rock's elastic properties and the orientation of the rock mass fabric with respect to the ground surface. For rock masses with horizontal planes of transverse anisotropy, the horizontal stress at a given depth below a ridge was found to increase with the ratio of horizontal to vertical Young's moduli, E_h/E_v, (or in other words as the rock mass deformability in the vertical direction increases). For the same ratio $E_h/E_v > 1$, horizontal stress is the greatest for ridges that have horizontal planes of transverse isotropy and the smallest for ridges with vertical planes of transverse isotropy. For valleys in rock masses with horizontal planes of transverse isotropy, the tensile region at the bottom of the valleys decreases as the ratio of horizontal to vertical moduli increases (again as the rock mass deformability in the vertical direction increases).

In a recent paper, Pan and Amadei [17] presented a new analytical method for determining the stress field in a homogeneous, general anisotropic and elastic half space subject to gravity and surface loads under a condition of generalized plane strain and limited by irregular (but smooth) outer boundaries. Using the closed-form solutions of Amadei and Pan [4] and the analytical function method of Lekhnitskii [18], expressions for the stresses in an anisotropic half space with an irregular outer boundary were derived. The stresses were found to depend on three analytical functions that can be determined using numerical conformal mapping [19] and an integral equation method [20].

In this paper the nature of the stress field in long anisotropic and symmetric ridges and valleys under gravity is considered. The rock mass is modeled as a linearly elastic, transversely isotropic and homogeneous continuum which deforms under a condition of plane strain. At the outset, the new analytical method of Pan and Amadei [17] is reviewed. Then, the method is used to determine gravity induced stresses in ridges and valleys in orthotropic and transversely istropic rock masses. Finally, a parametric study is presented on the effect of (1) topography, (2) orientation of anisotropy and (3) degree of anisotropy on the magnitude and distribution of gravitational stresses in transversely isotropic rock masses with planes of anisotropy striking parallel to the ridge or valley axis.

STATEMENT OF THE PROBLEM

Consider the equilibrium of an anisotropic half space with the geometry of Fig. 1. The half space represents a rock mass with an irregular topography which is subject to gravity only. The medium in the half space is assumed to be linearly elastic, homogeneous, anisotropic and continuous with a uniform density ρ. An x, y, z coordinate system is attached to the half space such that the x and z axes are in the horizontal plane and the y axis is pointing upward. The half space geometry and the medium's elastic properties are assumed to be independent of the z direction. The boundary curve of the half space is defined by an analytic function $y = y(x)$ or in parametric form $x = x(t)$, $y = y(t)$.

The problem is to find the magnitude and distribution of the stresses induced by gravitational loading of the half space. Since the geometry of the problem is indepen-

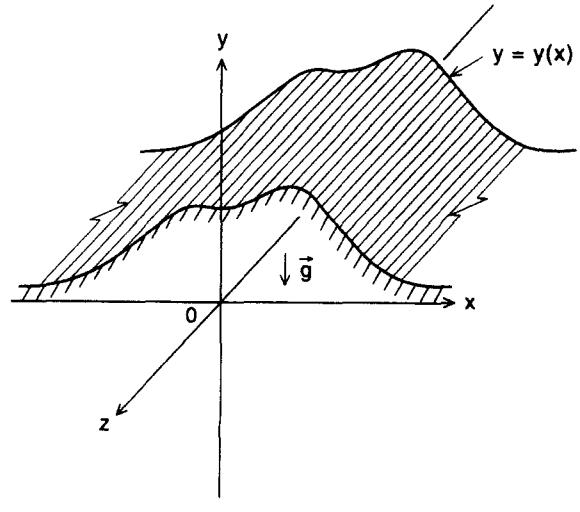

Fig. 1. Half space limited by a boundary curve $y = y(x)$ and subject to gravity **g**.

dent of the z coordinate and the medium is homogeneous, the stresses can be determined assuming a condition of generalized plane strain, e.g. all planes normal to the z axis are assumed to warp identically with $\epsilon_z = 0$ [18]. As $x \to \pm\infty$, the lateral horizontal strains ϵ_x and γ_{xz} approach zero. The stresses and strains induced by gravity must satisfy the following equations:

(i) Equations of equilibrium

$$\begin{aligned} \frac{\partial \sigma_{xx}}{\partial x} + \frac{\partial \sigma_{xy}}{\partial y} &= 0 \\ \frac{\partial \sigma_{xy}}{\partial x} + \frac{\partial \sigma_{yy}}{\partial y} + \rho g &= 0. \\ \frac{\partial \sigma_{xz}}{\partial x} + \frac{\partial \sigma_{yz}}{\partial y} &= 0. \end{aligned} \tag{1}$$

(ii) Constitutive relations

$$[\mathbf{e}] = [\mathbf{a}][\sigma] \tag{2}$$

or

$$[\sigma] = [\mathbf{c}][\mathbf{e}] \tag{3}$$

where

$$[\mathbf{e}] = [\epsilon_x, \epsilon_y, \epsilon_z, \gamma_{yz}, \gamma_{xz}, \gamma_{xy}]^T \tag{4}$$

are the strain components, and

$$[\sigma] = [\sigma_{xx}, \sigma_{yy}, \sigma_{zz}, \sigma_{yz}, \sigma_{xz}, \sigma_{xy}]^T \tag{5}$$

are the stress components, $[\mathbf{a}]$ is a 6×6 symmetric compliance matrix with 21 independent components a_{ij} $(i,j = 1\text{–}6)$ and $[\mathbf{c}]$ is the corresponding stiffness matrix with components c_{ij} $(i,j = 1\text{–}6)$ and is such that $[\mathbf{a}] = [\mathbf{c}]^{-1}$. In equations (4) and (5), the superscript T indicates the transpose of the matrix. In this paper, the rock mechanics sign convention that compressive stresses are positive is adopted.

(iii) Compatibility conditions

$$\begin{aligned} \frac{\partial \gamma_{xz}}{\partial y} - \frac{\partial \gamma_{yz}}{\partial x} &= 0 \\ \frac{\partial^2 \epsilon_x}{\partial y^2} + \frac{\partial^2 \epsilon_y}{\partial x^2} &= \frac{\partial^2 \gamma_{xy}}{\partial x\, \partial y}. \end{aligned} \tag{6}$$

(iv) Boundary conditions on $y = y(x)$

$$\begin{aligned} \sigma_{xx}\cos(n,x) + \sigma_{xy}\cos(n,y) &= 0 \\ \sigma_{xy}\cos(n,x) + \sigma_{yy}\cos(n,y) &= 0 \\ \sigma_{xz}\cos(n,x) + \sigma_{yz}\cos(n,y) &= 0 \end{aligned} \tag{7}$$

where $\cos(n,x)$ and $\cos(n,y)$ are the direction cosines of the outward normal, $\mathbf{n}$, of the boundary curve $y = y(x)$.

ANALYTICAL SOLUTION OF THE PROBLEM

Using the closed-form solutions of Amadei and Pan [4] for the gravitational stresses in anisotropic rock masses with a horizontal ground surface and the analytical function method of Lekhnitskii [18], Pan and Amadei [17] proposed the following expressions for the stresses in an anisotropic half space with an irregular boundary

$$\begin{aligned} \sigma_{xx} &= 2\,\mathrm{Re}[\mu_1^2\Phi_1'(z_1) + \mu_2^2\Phi_2'(z_2) + \mu_3^2\lambda_3\Phi_3'(z_3)] + c_1\rho g y \\ \sigma_{yy} &= 2\,\mathrm{Re}[\Phi_1'(z_1) + \Phi_2'(z_2) + \lambda_3\Phi_3'(z_3)] + \rho g y \\ \sigma_{xy} &= -2\,\mathrm{Re}[\mu_1\Phi_1'(z_1) + \mu_2\Phi_2'(z_2) + \mu_3\lambda_3\Phi_3'(z_3)] \\ \sigma_{xz} &= 2\,\mathrm{Re}[\mu_1\lambda_1\Phi_1'(z_1) + \mu_2\lambda_2\Phi_2'(z_2) + \mu_3\Phi_3'(z_3)] + c_2\rho g y \\ \sigma_{yz} &= -2\,\mathrm{Re}[\lambda_1\Phi_1'(z_1) + \lambda_2\Phi_2'(z_2) + \Phi_3'(z_3)] \\ \sigma_{zz} &= \frac{2}{a_{33}}\mathrm{Re}\{[a_{13}\mu_1^2 + a_{23} - a_{34}\lambda_1 + a_{35}\mu_1\lambda_1 \\ &\quad - a_{36}\mu_1]\Phi_1'(z_1) + [a_{13}\mu_2^2 + a_{23} - a_{34}\lambda_2 + a_{35}\mu_2\lambda_2 \\ &\quad - a_{36}\mu_2]\Phi_2'(z_2) + [a_{13}\lambda_3\mu_3^2 + a_{23}\lambda_3 - a_{34} + a_{35}\mu_3 \\ &\quad - a_{36}\mu_3\lambda_3]\Phi_3'(z_3)\} + c_3\rho g y. \end{aligned} \tag{8}$$

In equation (8):

(i) c_1, c_2 and c_3 are related to the coefficients c_{ij} of matrix $[\mathbf{c}]$ in equation (3) with

$$\begin{aligned} c_1 &= -[c_{12}(c_{44}c_{66} - c_{46}^2) - c_{14}(c_{24}c_{66} - c_{26}c_{46}) \\ &\quad + c_{16}(c_{24}c_{46} - c_{26}c_{44})]/D \\ c_2 &= -[c_{25}(c_{44}c_{66} - c_{46}^2) - c_{45}(c_{24}c_{66} - c_{26}c_{46}) \\ &\quad + c_{56}(c_{24}c_{46} - c_{26}c_{44})]/D \\ c_3 &= -[c_{23}(c_{44}c_{66} - c_{46}^2) - c_{34}(c_{24}c_{66} - c_{26}c_{46}) \\ &\quad + c_{36}(c_{24}c_{46} - c_{26}c_{44})]/D \end{aligned} \tag{9}$$

and

$$\begin{aligned} D &= c_{22}(c_{44}c_{66} - c_{46}^2) - c_{24}(c_{42}c_{66} - c_{62}c_{46}) \\ &\quad + c_{26}(c_{24}c_{46} - c_{26}c_{44}) \end{aligned} \tag{10}$$

(ii) μ_1, μ_2 and μ_3 are complex numbers with positive imaginary parts. These numbers and their respective conjugates are the roots of the following equation

$$l_4(\mu)l_2(\mu) - l_3^2(\mu) = 0 \tag{11}$$

with

$$\begin{aligned} l_2(\mu) &= \beta_{55}\mu^2 - 2\beta_{45}\mu + \beta_{44} \\ l_3(\mu) &= \beta_{15}\mu^3 - (\beta_{14} + \beta_{56})\mu^2 + (\beta_{25} + \beta_{46})\mu - \beta_{24} \\ l_4(\mu) &= \beta_{11}\mu^4 - 2\beta_{16}\mu^3 + (2\beta_{12} + \beta_{66})\mu^2 \\ &\quad - 2\beta_{26}\mu + \beta_{22} \end{aligned} \tag{12}$$

β_{ij} $(i,j = 1\text{–}6)$ are related to the coefficients a_{ij} of matrix $[\mathbf{a}]$ in equation (2) as follows

$$\beta_{ij} = a_{ij} - a_{i3}a_{j3}/a_{33} \quad (i,j = 1, 2, 4, 5, 6). \tag{13}$$

(iii) λ_1, λ_2 and λ_3 are such that

$$\lambda_1 = -\frac{l_3(\mu_1)}{l_2(\mu_1)}; \quad \lambda_2 = -\frac{l_3(\mu_2)}{l_2(\mu_2)}; \quad \lambda_3 = -\frac{l_3(\mu_3)}{l_4(\mu_3)}. \tag{14}$$

(iv) $\Phi_k'(z_k)$ $(k = 1, 2, 3)$ denote the derivatives of three analytical stress functions $\Phi_k(z_k)$ of the variable $z_k = x + \mu_k y$ where x and y are the coordinates of the point in the anisotropic medium at which the stresses are calculated. The three functions $\Phi_k(z_k)$ must satisfy the traction free boundary conditions along the boundary curve $y = y(x)$. These conditions can be expressed as follows

$$2\,\mathrm{Re}[\Phi_1(z_1) + \Phi_2(z_2) + \lambda_3\Phi_3(z_3)] = -\rho g \int_0^s yx'(s)\,ds \quad (15)$$

$$2\,\mathrm{Re}[\mu_1\Phi_1(z_1) + \mu_2\Phi_2(z_2) + \mu_3\lambda_3\Phi_3(z_3)] = -c_1\rho g \int_0^s yy'(s)\,ds \quad (16)$$

$$2\,\mathrm{Re}[\lambda_1\Phi_1(z_1) + \lambda_2\Phi_2(z_2) + \Phi_3(z_3)] = -c_2\rho g \int_0^s yy'(s)\,ds \quad (17)$$

where s is the arc-length along the curve $y = y(x)$. $x'(s)$ and $y'(s)$ are the total derivatives of x and y with respect to s, respectively.

The determination of the three functions $\Phi_k(z_k)$ and their derivatives depends mainly upon the geometry of the boundary curve $y = y(x)$. As shown by Pan and Amadei [17], these functions can be determined using a numerical conformal mapping method [19] and an integral equation method [20]. Three new analytical functions Ψ_k $(k = 1, 2, 3)$ are introduced such that

$$\Psi_k'(\zeta_k) = \Phi_k'(z_k)Z_k'(\zeta_k) \quad (k = 1, 2, 3) \quad (18)$$

where $z_k = Z_k(\zeta_k)$ $(k = 1, 2, 3)$ are three conformal mapping functions that map the lower half planes bounded by $z_k = x(t) + \mu_k y(t)$ onto the lower flat half planes $Im\,\zeta_k \leqslant 0$ $(k = 1, 2, 3)$. This is done in three steps [17]. First, the lower half planes bounded by $z_k = x(t) + \mu_k y(t)$ are mapped onto irregular bounded domains w_k. Then, the domains w_k are mapped onto unit disks F_k. Finally, the unit disks F_k are mapped onto the flat half planes ζ_k. In equation (18), $\Psi_k'(\zeta_k)$ and $Z_k'(\zeta_k)$ are the total derivatives of Ψ_k and Z_k with respect to ζ_k. As shown by Pan and Amadei [17], if t_k is the value of ζ_k on the boundary curve, the boundary conditions (15)–(17) lead to the following system of three singular integral equations that can be solved for the three functions $\Psi_k'(t_k)$

$$b_{11}\Psi_1'(\tau_1) + \frac{b_{12}}{2}\Psi_2'(\tau_2)t_2'(\tau_1) + \frac{b_{13}}{2}\Psi_3'(\tau_3)t_3'(\tau_1) + \frac{b_{12}}{2\pi i}\int_{+\infty}^{-\infty}\frac{\Psi_2'(t_2)t_2'(t_1)\,dt_1}{t_1 - \tau_1} + \frac{b_{13}}{3\pi i}\int_{+\infty}^{-\infty} \times \frac{\Psi_3'(t_3)t_3'(t_1)\,dt_1}{t_1 - \tau_1} = \frac{f_1(\tau)t'(\tau_1)}{2} + \frac{1}{2\pi i}\int_{+\infty}^{-\infty}\frac{f_1(t)t'(t_1)\,dt_1}{t_1 - \tau_1} \quad (19)$$

$$b_{21}\Psi_2'(\tau_2) + \frac{b_{22}}{2}\Psi_1'(\tau_1)t_1'(\tau_2) + \frac{b_{23}}{2}\Psi_3'(\tau_3)t_3'(\tau_2) + \frac{b_{22}}{2\pi i}\int_{+\infty}^{-\infty}\frac{\Psi_1'(t_1)t_1'(t_2)\,dt_2}{t_2 - \tau_2} + \frac{b_{23}}{2\pi i}\int_{+\infty}^{\infty} \times \frac{\Psi_3'(t_3)t_3'(t_2)\,dt_2}{t_2 - \tau_2} = \frac{f_2(\tau)t'(\tau_2)}{2} + \frac{1}{2\pi i}\int_{+\infty}^{-\infty}\frac{f_2(t)t'(t_2)\,dt_2}{t_2 - \tau_2} \quad (20)$$

$$b_{31}\Psi_3'(\tau_3) + \frac{b_{32}}{2}\Psi_1'(\tau_1)t_1'(\tau_3) + \frac{b_{33}}{2}\Psi_2'(\tau_2)t_2'(\tau_3) + \frac{b_{32}}{2\pi i}\int_{+\infty}^{-\infty}\frac{\Psi_1'(t_1)t_1'(t_3)\,dt_3}{t_3 - \tau_3} + \frac{b_{33}}{2\pi i}\int_{+\infty}^{-\infty} \times \frac{\Psi_2'(t_2)t_2'(t_3)\,dt_3}{t_3 - \tau_3} = \frac{f_3(\tau)t'(\tau_3)}{2} + \frac{1}{2\pi i}\int_{+\infty}^{-\infty}\frac{f_3(t)t'(t_3)\,dt_3}{t_3 - \tau_3} \quad (21)$$

where the coefficients b_{ij} $(i, j = 1, 2, 3)$ and the functions $f_i(t)$ $(i = 1, 2, 3)$ are given by equations (A1) and (A2) in the Appendix. In equations (19)–(21), τ is a fixed point on the t $[-\infty, +\infty]$ axis and τ_k $(k = 1, 2, 3)$ are fixed points on the t_k $(Im\,\zeta_k = 0)$ axes. $t'(t_j)$ and $t_k'(t_j)$ $(k, j = 1, 2, 3)$ are respectively the total derivatives of t and t_k with respect to the variable t_j $[-\infty, +\infty]$ and are equal to

$$t'(t_j) = \frac{Z_j'(t_j)}{x'(t) + \mu_j y'(t)};$$

$$t_k'(t_j) = \frac{Z_j'(t_j)}{Z_k'(t_k)} \cdot \frac{x'(t) + \mu_k y'(t)}{x'(t) + \mu_j y'(t)}. \quad (22)$$

In equation (22), $x'(t)$ and $y'(t)$ are the total derivatives of $x(t)$ and $y(t)$ with respect to t, respectively.

The three integral equations (19)–(21) can be discretized and solved for the boundary values of the three analytical functions $\Psi_k'(t_k)$ by the method proposed by Sarkar *et al.* [21]. Then, the interior values of these analytical functions are calculated using the Cauchy integral theorem [22]. Finally, the stress function $\Phi_k'(z_k)$ are obtained using equation (18) and the six stress components are determined using equation (8). The infinite integrals appearing in equations (19)–(21) are determined using an inverse mapping from the boundary of the ζ_k planes to the circumference of unit discs [17]. It is noteworthy that for these integrals to converge, the boundary curve $x = x(t)$, $y = y(t)$ must be asymptotic to the x-axis of Fig. 1 at $x = \pm\infty$ and the following conditions must be satisfied

$$\lim_{t \to \pm\infty} |y(t)x'(t)| = a_1 < \infty;$$

$$\lim_{t \to \pm\infty} |y(t)y'(t)| = a_2 < \infty \quad (23)$$

where a_1 and a_2 are two constants.

STRESSES IN AN ISOLATED RIDGE OR VALLEY

Generalized plane strain solution

Consider a long isolated symmetric ridge with the geometry of Fig. 2(a). The topography of the ridge is expressed in parametric form as follows

$$x(t) = t \quad (-\infty < t < +\infty)$$
$$y(t) = a^2 b/(t^2 + a^2) \tag{24}$$

where b is the ridge height and is assumed to be positive. If b is negative, equation (24) corresponds to a long isolated symmetric valley where $|b|$ is the depth of the valley [Fig. 2(b)]. The inflection points of the boundary curve are located at $x = \pm a/\sqrt{3}$ and $y = 0.75b$ at which the slopes are equal to $\pm(3b\sqrt{3})/(8a)$. Figures 3(a) and (b) show the geometry (in dimensionless form) of three ridges and valleys for $a/|b| = 0.5$, 1 and 2. The respective slopes at the inflection points of the ridges and valleys are equal to ± 1.30 (52.4°), ± 0.65 (33.0°) and ± 0.32 (18°).

For the geometry of Figs 2(a) and (b), the mappings $z_k = Z_k(\zeta_k)$ $(k = 1, 2, 3)$ which map the lower half planes bounded by $z_k = x(t) + \mu_k y(t)$ onto the flat lower half planes $Im\,\zeta_k \leqslant 0$ $(k = 1, 2, 3)$ consist of three successive conformal mappings (Fig. 4):

Mapping 1:

$$z_k \Rightarrow w_k \quad k = 1, 2, 3$$
$$w_k(t) = \frac{t + \dfrac{a^2 b\mu_k}{t^2 + a^2} + iA_k}{t + \dfrac{a^2 b\mu_k}{t^2 + a^2} - iA_k} \quad -\infty < t < \infty \tag{25}$$

maps the lower half planes bounded by $z_k = x(t) + \mu_k y(t)$ onto irregular bounded domains w_k. In equation (25), A_k $(k = 1, 2, 3)$ are complex constants

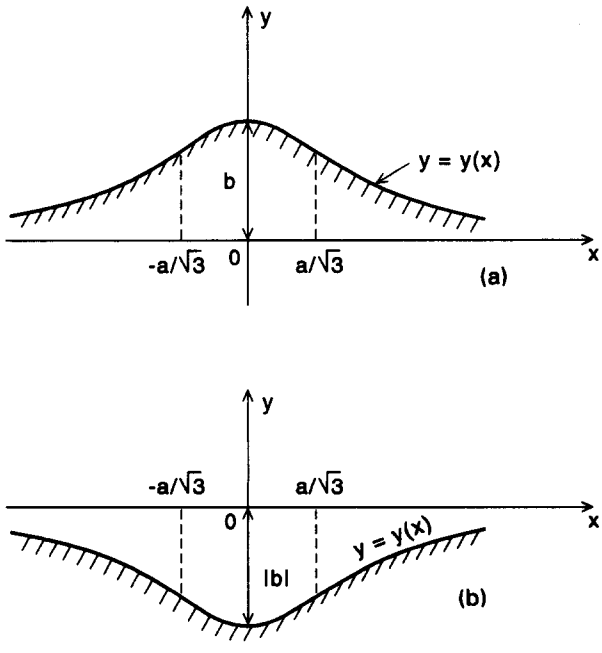

Fig. 2. (a) Symmetric ridge of height b; (b) symmetric valley of depth $|b|$.

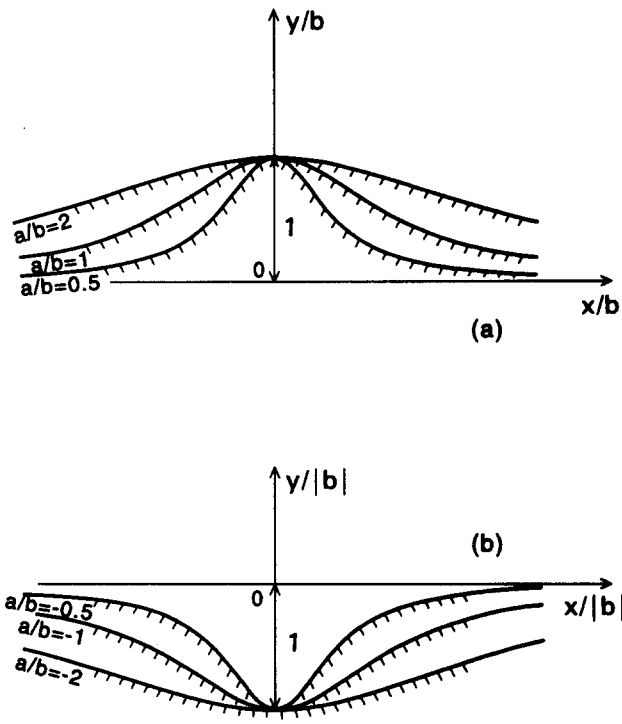

Fig. 3. Geometry of the ridge and valley for values of $a/|b|$ of 0.5, 1 and 2.

chosen such that the mapping is conformal. In equation (25), the variable t can be replaced by a new parameter θ that varies over a finite interval $[-\pi/2, \pi/2]$ such that $t = a \cdot \tan\theta$. Then equation (25) takes the following form

$$w_k(\theta) = \frac{a \cdot \sin\theta + b\mu_k \cos^3\theta + iA_k \cos\theta}{a \cdot \sin\theta + b\mu_k \cos^3\theta - iA_k \cos\theta}$$
$$k = 1, 2, 3; \quad -\frac{\pi}{2} < \theta < \frac{\pi}{2} \tag{26}$$

Mapping 2:

$$w_k \Rightarrow F_k \quad k = 1, 2, 3$$
$$F_k = F_k(w_k) \tag{27}$$

maps the irregular bounded domains w_k onto unit discs F_k. This is done using a numerical conformal mapping method as discussed in Trummer [19] and Pan and Amadei [17].

Mapping 3:

$$F_k \Rightarrow \zeta_k \quad k = 1, 2, 3$$
$$\zeta_k = i\frac{F_k(w_k) + 1}{F_k(w_k) - 1} \tag{28}$$

maps the unit discs F_k onto the flat half-planes ζ_k.

For the geometry of Figs 2(a) and (b), $t'(t_j)$ and $t'_k(t_j)$ defined in equation (22) take the following form

$$t'(t_j) = \frac{Z'_j(t_j)}{1 - \dfrac{2a^2 bt\mu_j}{(a^2 + t^2)^2}}$$
$$t'_k(t_j) = \frac{Z'_j(t_j)}{Z'_k(t_k)} \cdot \frac{(a^2 + t^2)^2 - 2a^2 bt\mu_k}{(a^2 + t^2)^2 - 2a^2 bt\mu_j}. \tag{29}$$

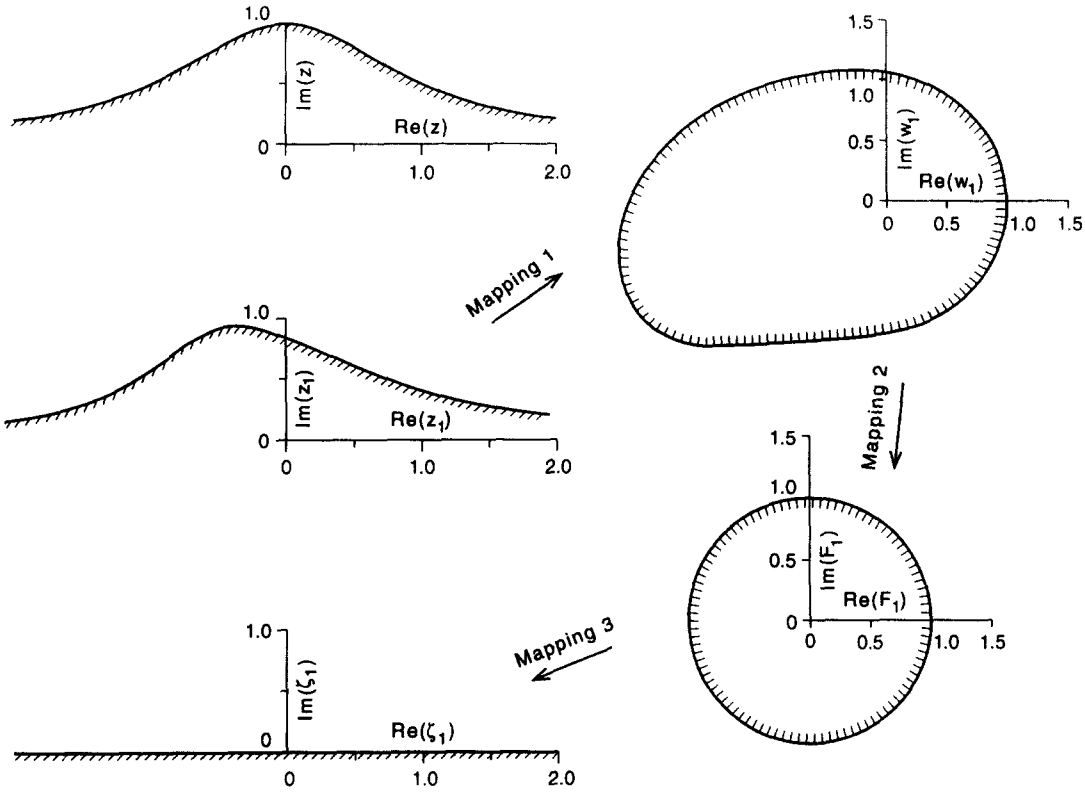

Fig. 4. Example of mappings 1, 2 and 3 for $k = 1$ and the following parameters: $a/b = 1$, $E/E' = G/G' = 3$, $\nu = 0.25$, $\nu' = 0.15$, and $\psi = 45°$.

The rock mass in the ridge or valley is assumed to be orthotropic in an n, s, t cartesian coordinate system. That coordinate system is attached to a plane of symmetry in the medium and its orientation with respect to the x, y, z coordinate system and therefore the ridge, is defined by a dip azimuth β and a dip angle ψ as shown in Fig. 5. The t-axis is located in the xz plane. The constitutive equation for the rock in the n, s, t coordinate system is given by the following equation [18]

coordinate system. E_n, E_s and E_t are the Young's moduli in the n, s, and t directions, respectively and G_{ns}, G_{nt} and G_{st} are the shear moduli in planes parallel to the ns, nt and st planes, respectively. Finally, ν_{ij} $(i, j = n, s, t)$ are the Poisson's ratios that characterize the normal strains in the symmetry directions j when a stress is applied in the symmetry directions i. Because of symmetry of the compliance matrix [**h**], Poisson's ratios ν_{ij} and ν_{ji} are such that $\nu_{ij}/E_i = \nu_{ji}/E_j$.

$$\begin{bmatrix} \epsilon_n \\ \epsilon_s \\ \epsilon_t \\ \gamma_{st} \\ \gamma_{nt} \\ \gamma_{ns} \end{bmatrix} = \begin{bmatrix} \frac{1}{E_n} & -\frac{\nu_{sn}}{E_s} & -\frac{\nu_{tn}}{E_t} & 0 & 0 & 0 \\ -\frac{\nu_{ns}}{E_n} & \frac{1}{E_s} & -\frac{\nu_{ts}}{E_t} & 0 & 0 & 0 \\ -\frac{\nu_{nt}}{E_n} & -\frac{\nu_{st}}{E_s} & \frac{1}{E_t} & 0 & 0 & 0 \\ 0 & 0 & 0 & \frac{1}{G_{st}} & 0 & 0 \\ 0 & 0 & 0 & 0 & \frac{1}{G_{nt}} & 0 \\ 0 & 0 & 0 & 0 & 0 & \frac{1}{G_{ns}} \end{bmatrix} \begin{bmatrix} \sigma_{nn} \\ \sigma_{ss} \\ \sigma_{tt} \\ \sigma_{st} \\ \sigma_{nt} \\ \sigma_{ns} \end{bmatrix} \tag{30}$$

or in a more complex matrix form as

$$[\mathbf{e}]_{nst} = [\mathbf{h}][\sigma]_{nst}. \tag{31}$$

Nine independent elastic constants are needed to describe the deformability of the rock in the n, s, t

Equations (30) and (31) still apply if the medium is transversely isotropic in one of the three ns, nt or st planes. In that case, only five independent elastic constants are needed to describe the deformability of the medium in the n, s, t coordinate system. Let's call these

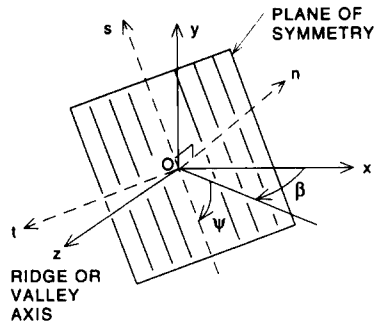

Fig. 5. Orientation of a plane of symmetry with respect to the x, y, z coordinate system attached to the ridge or valley.

constants E, E', ν, ν' and G' with the following definitions:

(i) E and E' are, respectively, Young's moduli in the plane of transverse istropy and in the direction normal to it,
(ii) ν and ν' are Poisson's ratios characterizing the lateral strain response in the plane of transverse isotropy to a stress acting parallel and normal to it, respectively, and,
(iii) G' is the shear modulus in planes normal to the plane of transverse isotropy.

Relationship exist between E, E', ν, and ν' and G' and the coefficients of matrix [**h**] in equation (31). For instance, for transverse isotropy in the st plane

$$\frac{1}{E_n}=\frac{1}{E'};\quad \frac{1}{E_s}=\frac{1}{E_t}=\frac{1}{E};\quad \frac{1}{G_{ns}}=\frac{1}{G_{nt}}=\frac{1}{G'}$$
$$\frac{\nu_{ns}}{E_n}=\frac{\nu_{nt}}{E_n}=\frac{\nu'}{E'};\quad \frac{\nu_{st}}{E_s}=\frac{\nu_{ts}}{E_t}=\frac{\nu}{E};\quad \frac{1}{G_{st}}=\frac{1}{G}=\frac{2(1+\nu)}{E}. \tag{32}$$

For known orientations of the planes of anisotropy with respect to the x, y and z axes, the constitutive relation of the medium in the x, y, z coordinate system defined in equation (2) or (3) can be obtained by using second order tensor coordinate transformation rules. Because of the linear relationships existing between coefficients a_{ij} and h_{ij} of matrices [**a**] and [**h**] in equations (2) and (31), respectively, it can be shown that the ratios between the stresses σ_{ij} defined in (8) and a characteristic stress $\rho g|b|$ depend on the following eight dimensionless quantities

$$\frac{E_s}{E_n};\quad \frac{E_s}{E_t};\quad \nu_{sn};\quad \nu_{tn};\quad \nu_{ts};\quad \frac{E_s}{G_{st}};\quad \frac{E_s}{G_{nt}};\quad \frac{E_s}{G_{ns}}. \tag{33}$$

If the medium is transversely isotropic with, for instance, transverse isotropy in the st plane, and using equation (32), the stress ratios are found to depend only on four dimensionless terms

$$\frac{E}{E'};\quad \nu;\quad \nu';\quad \frac{G}{G'}. \tag{34}$$

The stress ratios $\sigma_{ij}/\rho g|b|$ also depend on (1) the orientation angles β and ψ of the planes of transverse isotropy with respect to the x, y and z axes attached to the ridge or valley, (2) the coordinates $(x/|b|, y/|b|)$ of the points at which the stresses are calculated and (3) the ratios $a/|b|$ and $b/|b|$ describing the geometry of the ridge or valley. Equation (8) shows that, in general, at each point in the half space the stress field is three-dimensional and the principal stress components are inclined with respect to the x, y and z axes attached to the ridge or valley.

Plane strain solution

The solution presented above takes a simpler form for orthotropic and transversely isotropic rock masses with planes of elastic symmetry normal to the z axis of Figs 2(a) and (b). This takes place (1) when the dip azimuth β in Fig. 5 is zero and the dip angle ψ varies between 0 and 90° or (2) when β and ψ are equal to 90°. For those cases the generalized plane strain solution reduces to a plane strain solution with

$$c_{46}=c_{56}=c_{4i}=c_{5i}=0 \quad \text{for } i=1,2,3$$
$$\beta_{46}=\beta_{56}=\beta_{4i}=\beta_{5i}=0 \quad \text{for } i=1,2,3$$
$$l_3(\mu)=\lambda_1=\lambda_2=\lambda_3=0 \tag{35}$$

Substituting these relations into the general solution, it is found that c_2 in the expression of σ_{xz} and the function $\Phi_3'(z_3)$ in equation (8) always vanish. The stress components are then equal to

$$\sigma_{xx}=2\,\mathrm{Re}[\mu_1^2\Phi_1'(z_1)+\mu_2^2\Phi_2'(z_2)]+c_1\rho gy$$
$$\sigma_{yy}=2\,\mathrm{Re}[\Phi_1'(z_1)+\Phi_2'(z_2)]+\rho gy$$
$$\sigma_{xy}=-2\,\mathrm{Re}[\mu_1\Phi_1'(z_1)+\mu_2\Phi_2'(z_2)]$$
$$\sigma_{xz}=\sigma_{yz}=0$$
$$\sigma_{zz}=-\frac{2}{a_{33}}\mathrm{Re}\{[a_{13}\mu_1^2+a_{23}-a_{36}\mu_1]\Phi_1'(z_1)+[a_{13}\mu_2^2+a_{23}-a_{36}\mu_2]\Phi_2'(z_2)\}+c_3\rho gy \tag{36}$$

where μ_1 and μ_2 are the roots of $l_4(\mu)=0$ in equation (12) and

$$\Phi_1'(z)=\Psi_1'(\zeta_1)/Z_1'(\zeta_1);\quad \Phi_2'(z_2)=\Psi_2'(\zeta_2)/Z_2'(\zeta_2). \tag{37}$$

The boundary values of the two functions Ψ_1' and Ψ_2', e.g. $\Psi_1'(t_1)$ and $\Psi_2'(t_2)$, are obtained by solving the two integral equations (19) and (20) with b_{ij} and $f_i(t)$ defined in equations (A3) and (A4) in the Appendix. Equation (36) shows that at each point in the ridge or valley, two of the three principal stresses induced by gravity are located in the x, y plane normal to the ridge or valley axis and that the longitudinal stress σ_{zz} is the third principal stress.

PARAMETRIC STUDY

In order to illustrate the analytical method presented above, a parametric study was carried out to assess the combined effect of rock anisotropy and topography on the magnitude and distribution of gravitational stresses below long and symmetric ridges or valleys under a plane strain condition. In the parametric study, the geometry of Figs 2(a), 2(b) and 5 is adopted with planes of transverse isotropy parallel to the ridge or valley axis

($\beta = 0°$). The following parameters are varied: the geometry of the ridges or valleys defined by the ratio $a/|b|$, the dip angle ψ of the planes of transverse isotropy, and the degree of rock anisotropy defined by the values of E/E', G/G', ν and ν'. The topographic ratio $a/|b|$ is taken equal to 0.5, 1 or 2 corresponding to ridges and valleys with slopes at their inflection points equal to ± 1.30 (52.4°), ± 0.65 (33.0°) and ± 0.32 (18°), respectively. The dip angle ψ varies between 0° (horizontal planes of transverse isotropy) and 90° (vertical planes of transverse isotropy). Finally, E/E' and G/G' vary between 1 and 3, the Poisson's ratio ν' varies between 0.15 and 0.35 and $\nu = 0.25$. In selecting the elastic constants of the transversely isotropic rock, the following equations must always be satisfied [1, 23]

$$E, E', G, G' > 0$$
$$0 \leqslant \nu < 1 \tag{38}$$
$$1 - \nu - 2\nu'^2 \frac{E}{E'} > 0.$$

Note that the anisotropic solution presented in this paper becomes singular if the rock mass is isotropic with $E/E' = G/G' = 1$ and $\nu = \nu'$ [17]. This is because the formulation for isotropic elasticity is different from that for anisotropic media as discussed by Lekhnitskii [18]. The isotropic case can however, be approached asymptotically by considering a near isotropic rock with $E/E' = G/G' = 1$, $\nu = 0.25$ and $\nu' = 0.24$ and $\psi = 0°$.

The results of the parametric study are presented below using trajectories and contours of dimensionless stresses $\sigma_1/\rho g|b|$ and $\sigma_2/\rho g|b|$ where σ_1 and σ_2 are the maximum and minimum in-plane principal stresses in the x, y plane normal to the ridge or valley axis. The variation of the dimensionless horizontal stress $\sigma_{xx}/\rho g|b|$ with $y/|b|$ along the ridge or valley centerline ($x/|b| = 0$) is also used in the parametric study. Note that when $\psi = 0°$ and 90° and for the nearly isotropic case, only the right halves of the plots of stress trajectories and contours are presented because of symmetry.

Figures 6(a)–(h) show the gravitational stress regime for a ridge and a valley with $a/|b| = 1$ in a nearly isotropic rock mass. As expected, the principal stresses in Figs 6(a) and (b) are no longer horizontal and vertical as in flat ground but are oriented parallel and normal to the ground surface along the boundary of the ridge and valley and gradually turn to become horizontal and vertical with depth. Figure 6(c) indicates that the largest value of the maximum compressive principal stress $\sigma_1/\rho g|b|$ is reached on the sides of the ridge (0.647 at $x/|b| = \pm 0.925$). For the ridge, the contours of the minimum compressive stress $\sigma_2/\rho g|b|$ tend to follow the ridge shape [Fig. 6(d)]. For the valley, Figures 6(e) and (f) indicate that there is a concentration of tensile stress $\sigma_2/\rho g|b|$ at the valley bottom (-0.98 at $x/|b| = 0$) and that the maximum stress $\sigma_1/\rho g|b|$ is compressive with contours that follow the valley shape. The depth of the tensile region below the valley bottom is about 0.4 times the valley depth [Fig. 6(b)]. Figures 6(g) and (h) show the variation of the vertical stress $\sigma_{yy}/\rho g|b|$ and the horizontal stresses $\sigma_{xx}/\rho g|b|$ and $\sigma_{zz}/\rho g|b|$ with $y/|b|$ along the ridge and valley centerline ($x/|b| = 0$). The short dashed lines in those two figures represent the variation of the standard vertical and horizontal stresses for the case when $b = 0$; i.e. when the ground surface is flat [4]. The topographically induced stresses in the ridge and valley become, with increasing depth, asymptotic to the standard stresses. The horizontal stresses σ_{xx} and σ_{zz} are slightly different and are both less than the vertical stress σ_{yy} except near the ridge crest where σ_{xx} is larger than σ_{yy} and σ_{zz}. The stress variations shown in Figs 6(g) and (h) are virtually identical to those given by Savage *et al.* (Figs 9 and 10 in Ref. [11]) for the isotropic case when the Poisson's ratio is 0.25.

Figures 7(a)–(h) show the gravitational stress regime for a ridge and a valley with $a/|b| = 1$ in a transversely isotropic rock mass with $E/E' = G/G' = 3$, $\nu = 0.25$ and $\nu' = 0.15$ with vertical planes of transverse isotropy ($\psi = 90°$). This represents a strongly anisotropic rock [1]. In general, the trends observed in Figs 6(a)–(h) can also be found in Figs 7(a)–(h), in particular compression in the ridge crest and concentration of $\sigma_1/\rho g|b|$ on the sides of the ridge (0.33 at $x/|b| = \pm 0.94$). Tensile stresses develop at the valley bottom with $\sigma_2/\rho g|b| = -0.51$ at $x/|b| = 0$. Comparison of Figs 7(g) and (h) with Figs 6(g) and (h) shows that the variations of the vertical stress $\sigma_{yy}/\rho g|b|$ and the horizontal stress $\sigma_{xx}/\rho g|b|$ and $\sigma_{zz}/\rho g|b|$ with depth along the ridge and valley centerlines for the transversely isotropic case differ from those in the nearly isotropic case. For the ridge and the valley with vertical planes of transverse isotropy, the stress regime is $\sigma_{xx} < \sigma_{zz} < \sigma_{yy}$ except near the ridge crest. Also, the horizontal stress σ_{xx} is always less compressive than the horizontal stress in the nearly isotropic case except near the valley bottom. On the other hand, the isotropic and anisotropic values of the longitudinal and vertical stresses σ_{zz} and σ_{yy} for the anisotropic and nearly isotropic cases differ only slightly.

Effect of dip angle and degree of rock anisotropy

Figures 8 and 9 show respectively the stress regimes for a ridge and a valley with $a/|b| = 1$ in transversely isotropic rock with $E/E' = G/G' = 3$, $\nu = 0.25$, $\nu' = 0.15$ and planes of transverse isotropy dipping at angles $\psi = 0$, 45 and 90°. Figures 8(d) and 9(d) show that at a given depth, the horizontal stress $\sigma_{xx}/\rho g|b|$ decreases as the dip angle increases. This stress is the greatest for ridges and valleys with horizontal planes of transverse isotropy ($\psi = 0°$) and the smallest for ridges and valleys with vertical planes of transverse isotropy ($\psi = 90°$). The effect of the dip angle on $\sigma_{xx}/\rho g|b|$ becomes dominant for values of $y/|b|$ less than 0.0 for ridges and -1.5 for valleys. Figures 8(a), 8(c), 9(a) and 9(c) show that the principal stresses adjust to the horizontal and vertical directions more rapidly with depth when $\psi = 90°$ than when $\psi = 0°$. Note that in Figs 8(b) and 9(b) because of the inclined anisotropy ($\psi = 45°$), the principal stress trajectories and the tensile region are no longer symmetric with respect to the vertical axial planes of the ridge and valley. For the valley, the largest tensile stress

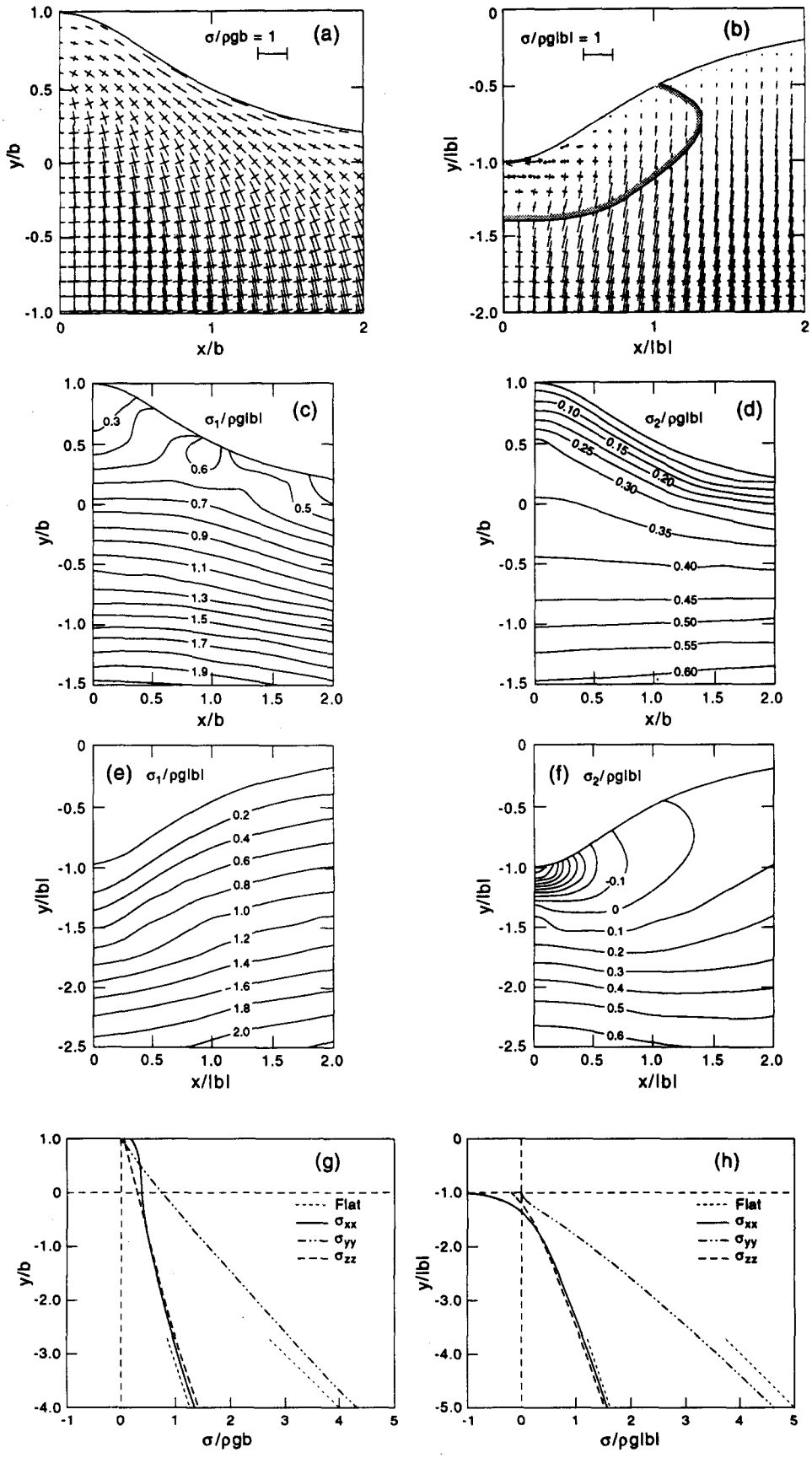

Fig. 6. Gravitational stress regime for a ridge and a valley with $a/|b| = 1$ in a nearly isotropic rock mass ($E/E' = G/G' = 1$, $\nu = 0.25$, $\nu' = 0.24$ and $\psi = 0°$). Stress trajectories for the ridge in (a) and the valley in (b), $\sigma_1/\rho g|b|$ and $\sigma_2/\rho g|b|$ stress contours for the ridge in (c) and (d) and for the valley in (e) and (f). Variation of $\sigma_{xx}/\rho g|b|$, $\sigma_{zz}/\rho g|b|$ and $\sigma_{yy}/\rho g|b|$ with $y/|b|$ along the ridge and valley centerline ($x/|b| = 0$) in (g) and (h). The short dashed lines in (g) and (h) represent the variation of the standard stresses in the absence of topography as proposed by Amadei and Pan [4]. The shaded region in (b) represents the extent of the tensile region at the valley bottom.

$\sigma_2/\rho g|b|$ is at the valley bottom and is equal to -1.4 and -0.52 for $\psi = 0$ and 90°, respectively. For $\psi = 45°$, it is on the valley left hand side ($x/|b| = -0.27$) and is equal to -0.71.

Figures 10 and 11 give the variation of $\sigma_{xx}/\rho g|b|$ with $y/|b|$ along the centerline of a transversely isotropic ridge and valley for $a/|b| = 1$ with $\nu = 0.25$, $\nu' = 0.15$ and values of E/E' and G/G' of 1 and 3. The planes of transverse isotropy dip at an angle $\psi = 0$, 45 and 90°. For a fixed value of E/E', Fig. 10 and 11 show that the value of the ratio G/G' has no effect on the variation of $\sigma_{xx}/\rho g|b|$ with depth for rock masses with horizontal and vertical planes of transverse isotropy. On the other hand, for planes of transverse isotropy dipping at 45°, the ratio G/G' has a strong effect where an increase in G/G' (as the rock mass becomes more deformable in shear in planes normal to the planes of transverse isotropy) results in an increase in $\sigma_{xx}/\rho g|b|$ and a decrease of the tensile region at the valley bottom. For a fixed value of G/G', Figs 10 and 11 show that E/E' affects the value of $\sigma_{xx}/\rho g|b|$ the most for horizontal anisotropy where $\sigma_{xx}/\rho g|b|$ increases with E/E' (or in other words as the rock mass becomes more deformable in the vertical direction). For vertical anisotropy, the effect of E/E' on

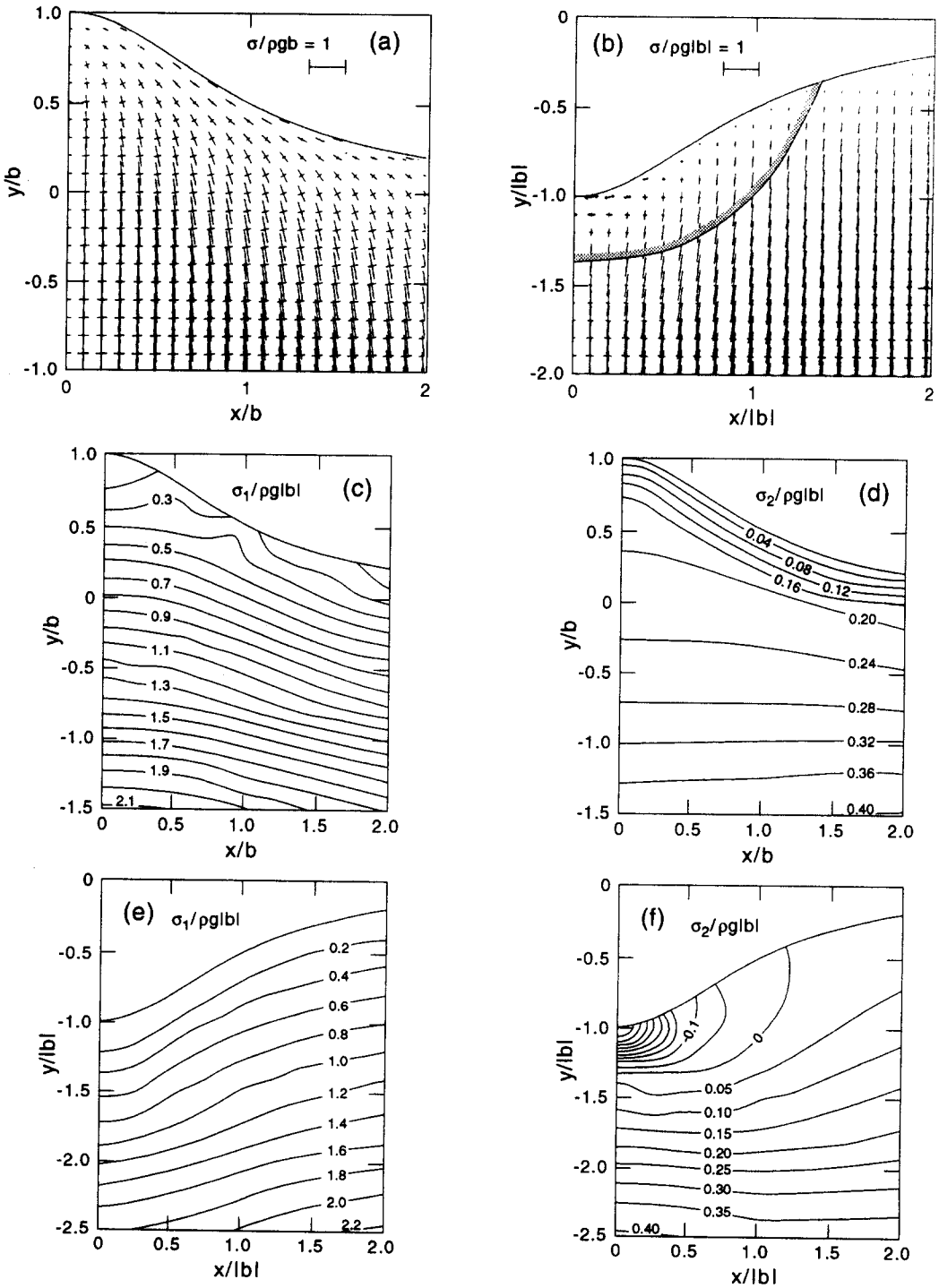

Fig. 7a, b, c, d, e and f. *Caption on facing page.*

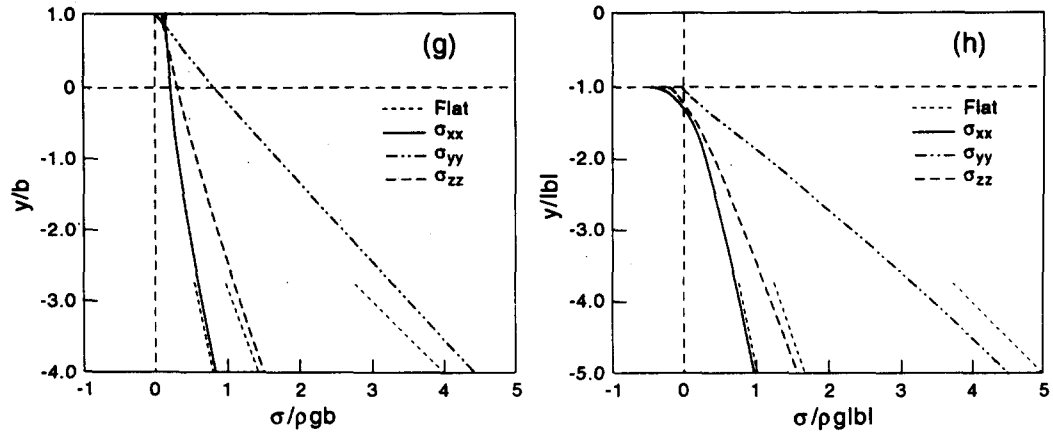

Fig. 7g and h.

Fig. 7. Gravitational stress regime for a ridge and a valley with $a/|b| = 1$ in a strongly transversely isotropic rock mass ($E/E' = G/G' = 3$, $\nu = 0.25$, $\nu' = 0.15$ and $\psi = 90°$). Stress trajectories for the ridge in (a) and the valley in (b), $\sigma_1/\rho g|b|$ and $\sigma_2/\rho g|b|$ stress contours for the ridge in (c) and (d) and for the valley in (e) and (f). Variation of $\sigma_{xx}/\rho g|b|$, $\sigma_{zz}/\rho g|b|$ and $\sigma_{yy}/\rho g|b|$ with $y/|b|$ along the ridge and valley centerline ($x/|b| = 0$) in (g) and (h). The short dashed lines in (g) and (h) represent the variation of the standard stresses in the absence of topography for this case of anisotropy [4]. The shaded region in (b) represents the extent of the tensile region at the valley bottom.

the magnitude of $\sigma_{xx}/\rho g|b|$ is small. For planes of anisotropy dipping at 45°, an increase in E/E' results in a decrease in $\sigma_{xx}/\rho g|b|$.

Figures 12 and 13 show the variation of $\sigma_{xx}/\rho g|b|$ with $y/|b|$ along the centerline of a transversely isotropic ridge and valley for $a/|b| = 1$ with $\nu = 0.25$, $E/E' = 3$, $G/G' = 1$ and for $\nu' = 0.15$, 0.25 and 0.35. The planes of transverse isotropy dip at an angle $\psi = 0$, 45 and 90°. At a given depth less than $y/|b| = 0$, the stress ratio $\sigma_{xx}/\rho g|b|$ increases with the Poisson's ratio ν'. For the valleys, the tensile region at the valley bottoms decreases as ν' increases and completely vanishes for $\nu' = 0.35$ for all dip angles.

Effect of ridge and valley geometry

Figures 14(a), (b) and (c) show the principal stress trajectories in transversely isotropic ridges with the topographic ratio $a/|b|$ equal to 0.5, 1 and 2, respectively. The ridges have horizontal planes of transverse isotropy ($\psi = 0°$) and are such that $E/E' = G/G' = 3$, $\nu = 0.25$ and $\nu' = 0.15$. The variation of the stress ratio $\sigma_1/\rho g|b|$ along the ground surface for the three ridges is shown in Fig. 15. We note from this figure that the maximum value of $\sigma_1/\rho g|b|$ increases with $a/|b|$ (0.747 for $a/|b| = 0.5$, 0.824 for $a/|b| = 1$ and 0.861 for $a/|b| = 2$) and that the location where the stress maximum is reached on the sides of the ridge moves further away from the ridge axis as $a/|b|$ increases or in other words as the ridge broadens. Also, the variation of $\sigma_1/\rho g|b|$ along the ground surface becomes gentler as $a/|b|$ increases. Figure 16 shows the variation of $\sigma_{xx}/\rho g|b|$ with $y/|b|$ along the centerline of the ridges for the three values of $a/|b|$. In this figure, an increase in $\sigma_{xx}/\rho g|b|$ with $a/|b|$ can be observed.

Figures 14 and 16 are replaced by Figs 17 and 18 for valleys in rock masses with horizontal planes of transverse isotropy, $a/|b| = 0.5$, 1 and 2, $E/E' = G/G' = 3$, $\nu = 0.25$ and $\nu' = 0.15$. Figures 17(a)–(c) show that the tensile region at the valley bottom increases as the valley broadens. More tension develops at the valley bottom as $a/|b|$ increases; ($\sigma_2/\rho g|b| = 0$ for $a/|b| = 0.5$, -0.79 for $a/|b| = 1$ and -1.33 for $a/|b| = 2$). In Fig. 18, the variation of $\sigma_{xx}/\rho g|b|$ with $y/|b|$ along the centerline of the valleys for the three values of $a/|b|$ shows a decrease in the horizontal stress with an increase in $a/|b|$.

As the ridges and valleys broaden, the ridge height or valley depth $|b|$ becomes zero, corresponding to a horizontal ground surface. Since the stresses are proportional to $|b|$ they approach the zero values predicted for a horizontal ground surface.

Depth of influence of topography

As shown above, the principal stress trajectories are oriented parallel and normal to the ground surface along the boundary of the ridge and valley and gradually turn to become horizontal and vertical with depth. In other words, the vertical stress component σ_{yy} and the horizontal stress components σ_{xx} and σ_{zz} tend to become principal stresses with depth and approach the values that they would have if the ground surface were horizontal. These latter stresses are defined as σ_{xxo}, σ_{yyo} and σ_{zzo}. The depth of influence of topography can be determined by calculating the ratios $R_{ii} = (\sigma_{ii} - \sigma_{iio})/\sigma_{iio}$ for $i = x$, y and z. As an example, Tables 1 and 2 give the values of $R_{xx} = (\sigma_{xx} - \sigma_{xxo})/\sigma_{xxo}$ at $y/|b| = -4.0$ and $x/|b| = 0$ and 3 for ridges and valleys in a near isotropic rock mass and a strongly anisotropic rock mass with $E/E' = G/G' = 3$, $\nu = 0.25$, $\nu' = 0.15$ and $\psi = 0$, 45 and 90°. Three ridge and valley geometries are considered with $a/|b| = 0.5$, 1 and 2.

Tables 1 and 2 indicate that broader ridges and valleys affect the stress field to a greater depth and to a wider area as expected. For a given ridge geometry, the effect of the topography on the stresses at depth is strongest for ridges and valleys in rock masses with vertical planes of transverse isotropy. The horizontal stress σ_{xx} approaches the standard stress σ_{xxo} more rapidly along the centerlines ($x/|b| = 0$) of the ridges and valleys than at

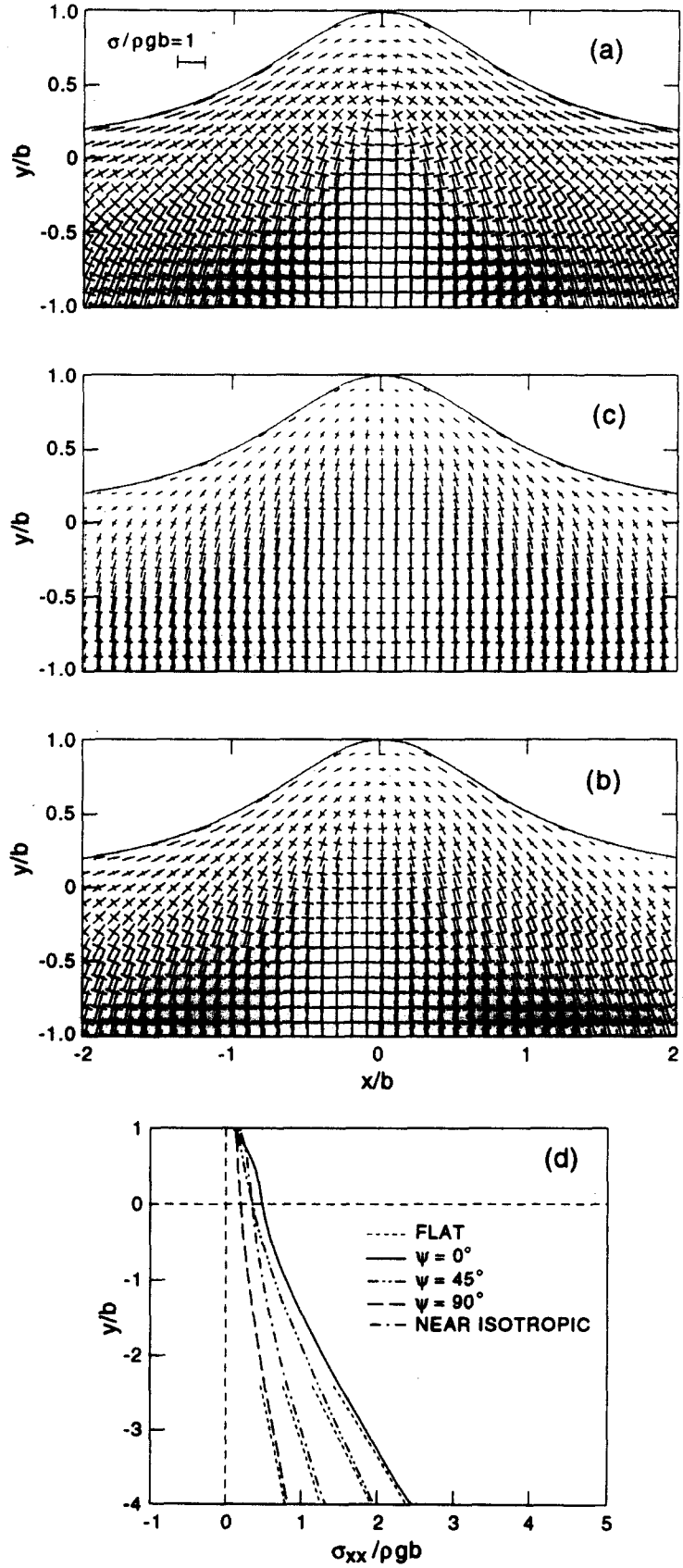

Fig. 8. Stress trajectories for a ridge with $a/b = 1$ in transversely isotropic rock with $E/E' = G/G' = 3$, $\nu = 0.25$, $\nu' = 0.15$ and $\psi = 0$, 45 and 90° in (a)–(c), respectively. Corresponding variations of $\sigma_{xx}/\rho g|b|$ with $y/|b|$ along the ridge centerline in (d). The short dashed lines in (d) represent the variation of the standard horizontal stress $\sigma_{xx}/\rho g|b|$ in the absence of topography for this case of anisotropy [4]. The variation of $\sigma_{xx}/\rho g|b|$ with $y/|b|$ for the nearly isotropic case is also shown for comparison in (d).

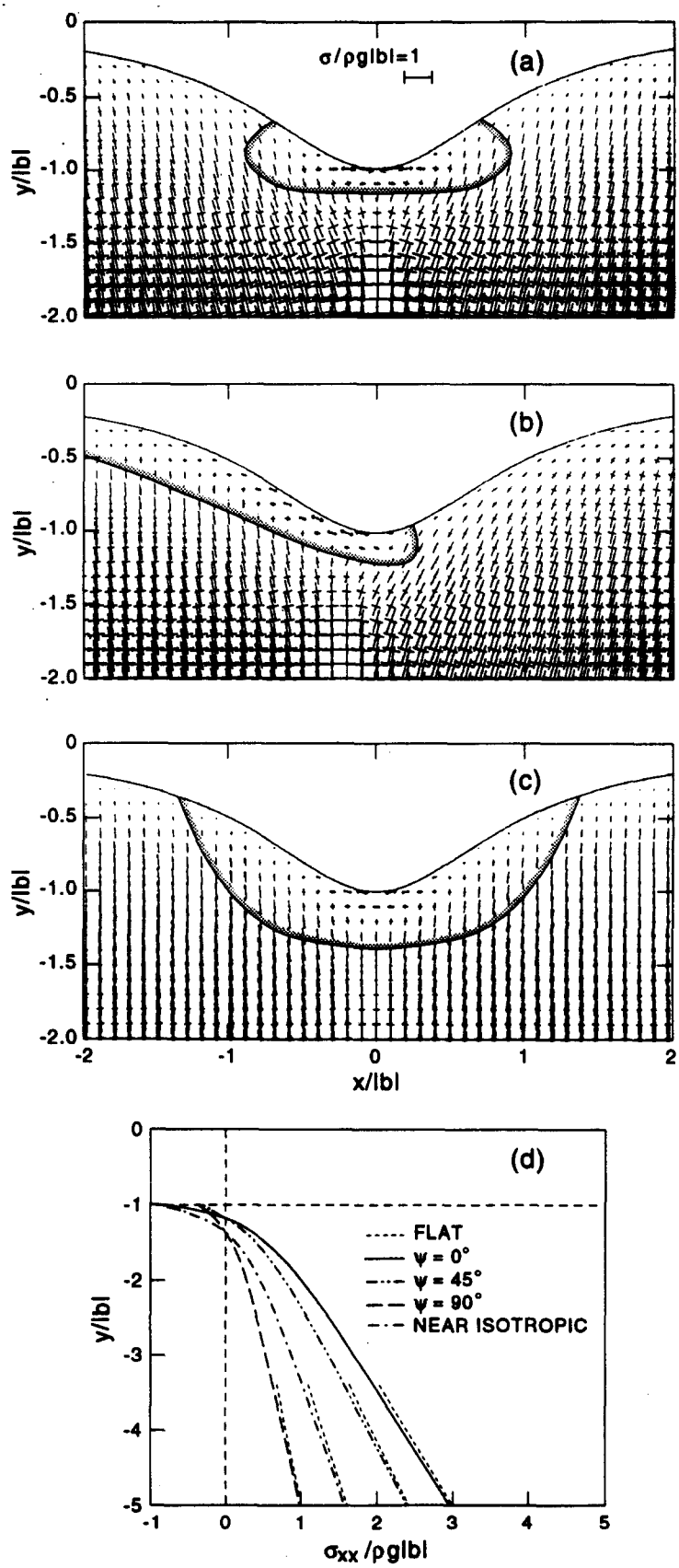

Fig. 9. Stress trajectories for a valley with $a/|b| = 1$ in transversely isotropic rock with $E/E' = G/G' = 3$, $\nu = 0.25$, $\nu' = 0.15$ and $\psi = 0$, 45 and 90° in (a)–(c), respectively. Corresponding variations of $\sigma_{xx}/\rho g|b|$ with $y/|b|$ along the valley centerline in (d). The short dashed lines in (d) represent the variation of the standard horizontal stress $\sigma_{xx}/\rho g|b|$ in the absence of topography for this case of anisotropy [4]. The variation of $\sigma_{xx}/\rho g|b|$ with $y/|b|$ for the nearly isotropic case is also shown for comparison in (d). The shaded regions in (a)–(c) represent the extent of the tensile region at the valley bottom.

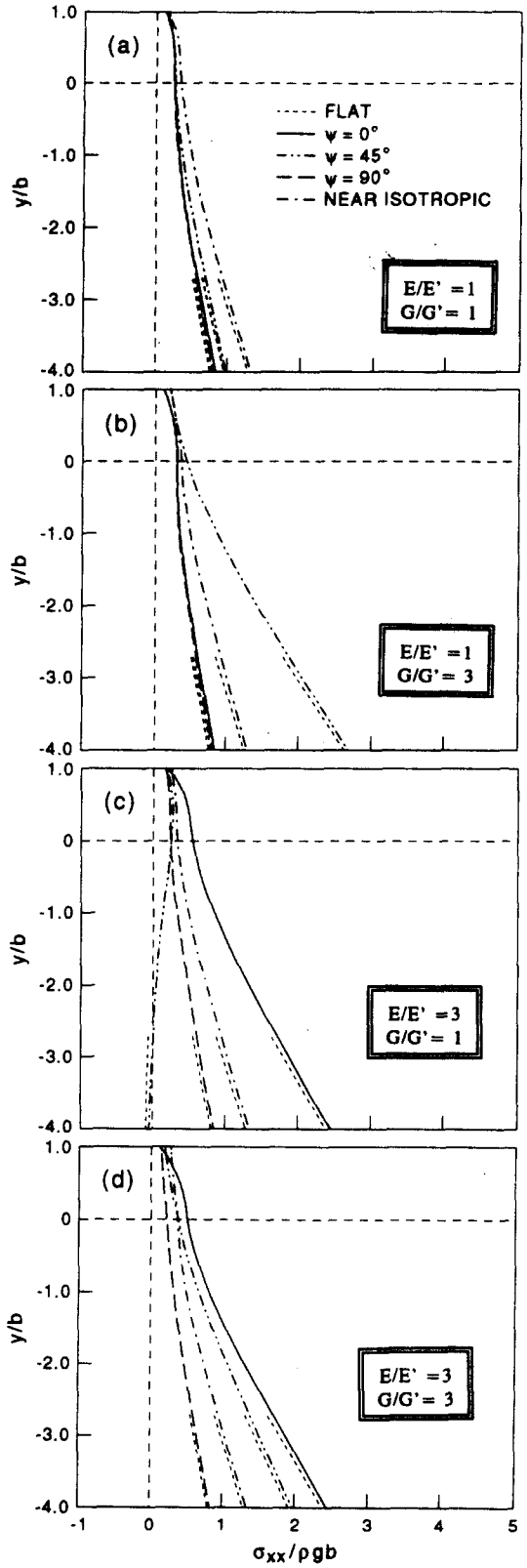

Fig. 10. Variation of $\sigma_{xx}/\rho g|b|$ with $y/|b|$ along the centerline of a ridge with $a/|b| = 1$ for transversely isotropic rock with $\nu = 0.25$, $\nu' = 0.15$. (a) $E/E' = G/G' = 1$; (b) $E/E' = 1$, $G/G' = 3$; (c) $E/E' = 3$, $G/G' = 1$; (d) $E/E' = G/G' = 3$. The planes of transverse isotropy dip at an angle $\psi = 0$, 45 and 90°. The nearly isotropic case is also shown for comparison. The short dashed lines in (a)–(d) represent the variation of the standard horizontal stress $\sigma_{xx}/\rho g|b|$ in the absence of topography for this case of anisotropy [4].

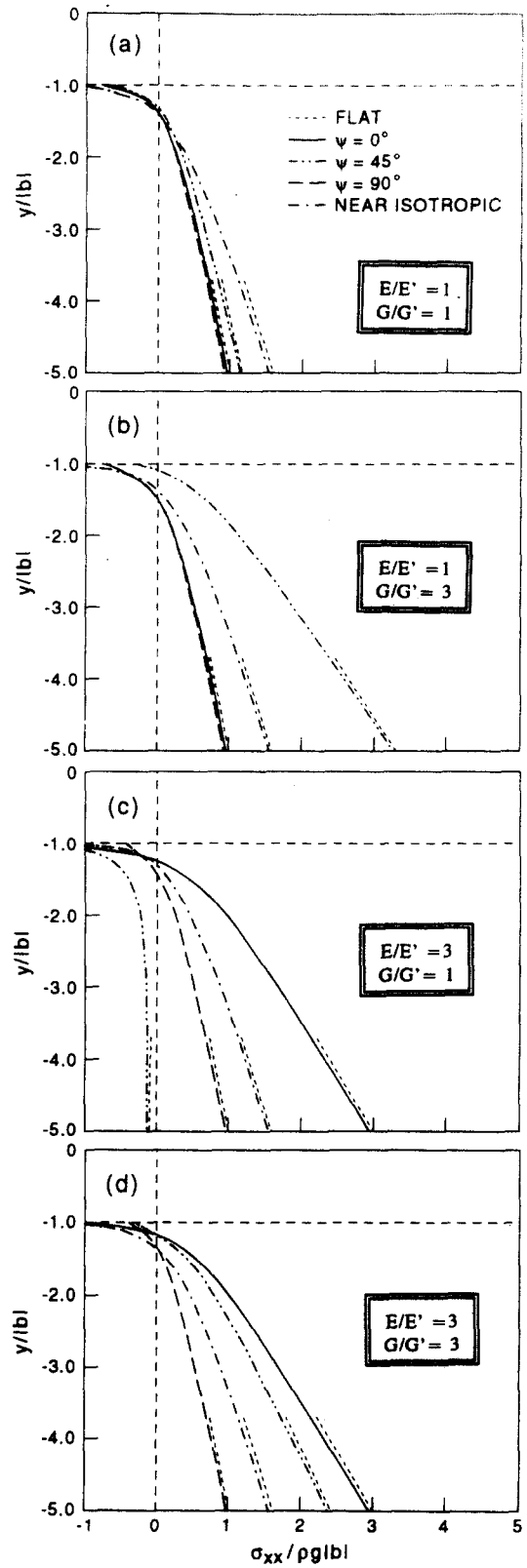

Fig. 11. Variation of $\sigma_{xx}/\rho g|b|$ with $y/|b|$ along the centerline of a valley with $a/|b| = 1$ for transversely isotropic rock with $\nu = 0.25$, $\nu' = 0.15$. (a) $E/E' = G/G' = 1$; (b) $E/E' = 1$, $G/G' = 3$; (c) $E/E' = 3$, $G/G' = 1$; (d) $E/E' = G/G' = 3$. The planes of transverse isotropy dip at an angle $\psi = 0$, 45 and 90°. The nearly isotropic case is also shown for comparison. The short dashed lines in (a)–(d) represent the variation of the standard horizontal stress $\sigma_{xx}/\rho g|b|$ in the absence of topography for this case of anisotropy [4].

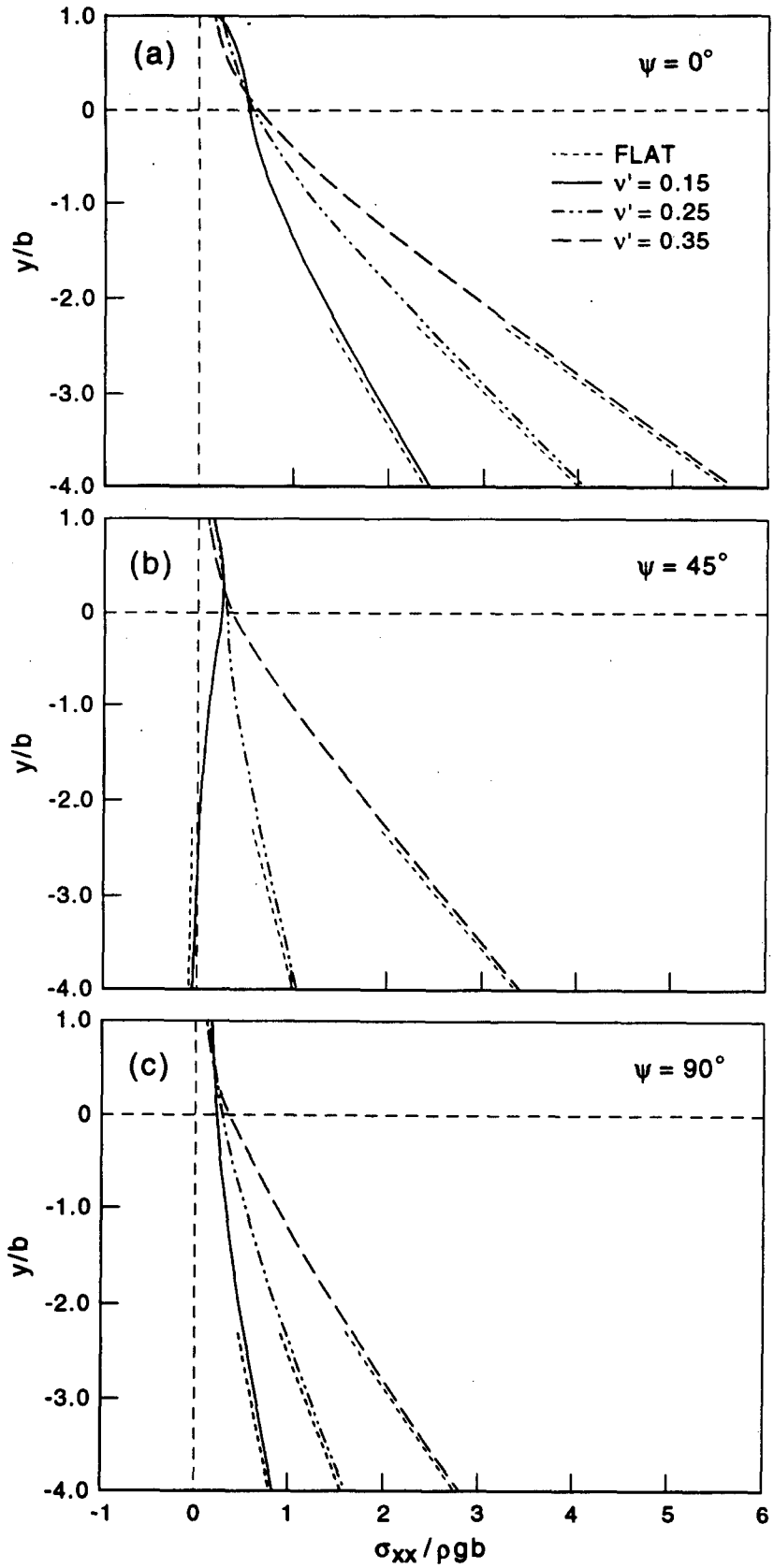

Fig. 12. Variation of $\sigma_{xx}/\rho g|b|$ with $y/|b|$ along the centerline of a ridge with $a/|b| = 1$ for transversely isotropic rock with $\nu = 0.25$, $E/E' = 3$ and $G/G' = 1$ and $\nu' = 0.15$, 0.25 and 0.35. (a) $\psi = 0$; (b) $\psi = 45$; and (c) $\psi = 90$. The short dashed lines in (a)–(c) represent the variation of the standard horizontal stress $\sigma_{xx}/\rho g|b|$ in the absence of topography for this case of anisotropy [4].

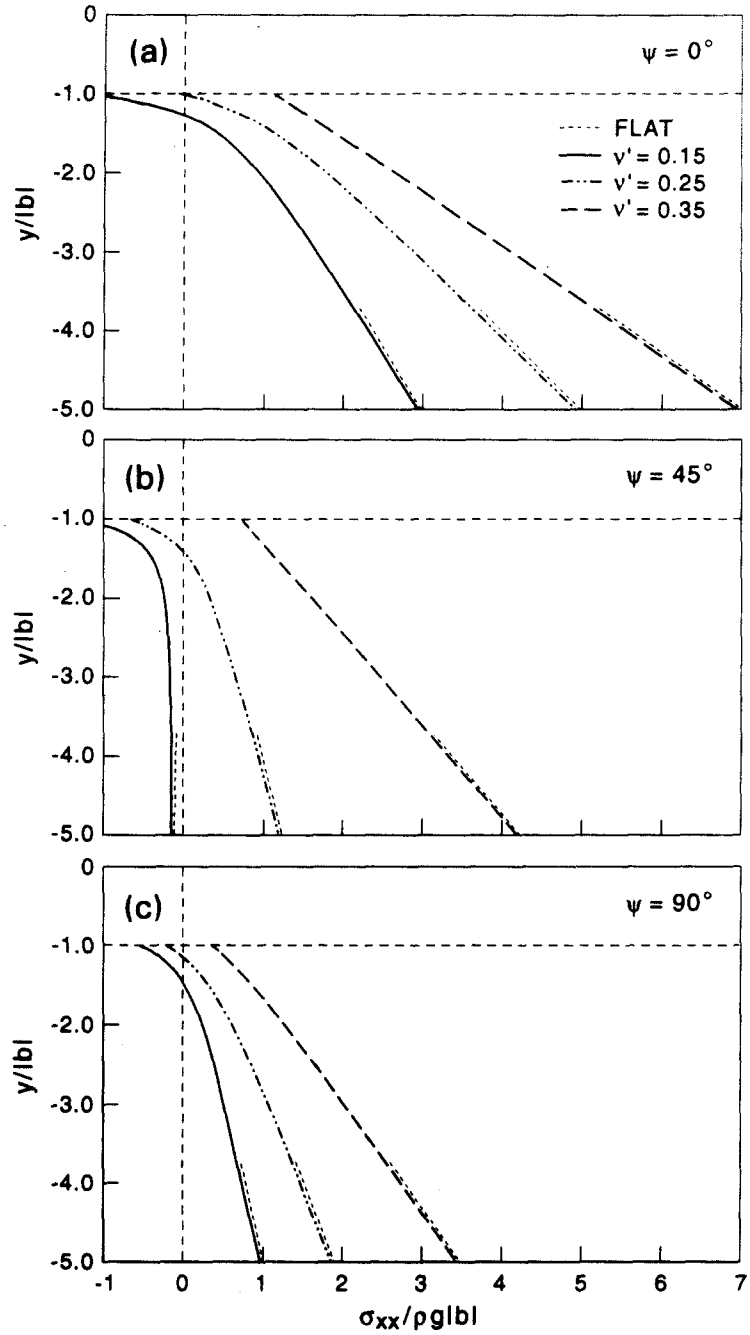

Fig. 13. Variation of $\sigma_{xx}/\rho g|b|$ with $y/|b|$ along the centerline of a valley with $a/|b| = 1$ for transversely isotropic rock with $\nu = 0.25$, $E/E' = 3$ and $G/G' = 1$ and $\nu' = 0.15$, 0.25 and 0.35. (a) $\psi = 0$; (b) $\psi = 45$; and (c) $\psi = 90$. The short dashed lines in (a)–(c) represent the variation of the standard horizontal stress $\sigma_{xx}/\rho g|b|$ in the absence of topography for this case of anisotropy [4].

$x/|b| = 3$. At $y/|b| = -4$ and for given values of $a/|b|$ and the dip angle ψ, the effect of the valley on the stresses is larger than the effect of the ridge.

Tensile region at valley bottoms

As shown in the numerical examples presented above, the extent of the tensile region at the valley bottom and the magnitude of the tensile stresses depend on parameters such as the ridge and valley geometry, the orientation of the anisotropy with respect to the ridge and valley axis and the degree of rock anisotropy. The following trends can be drawn:

- For a given set of rock elastic properties and a given valley geometry, the extent of the tensile region depends strongly on the dip angle ψ. This is shown in Figs 19(a) and (b) for a valley in a rock mass with $E/E' = G/G' = 3$, $\nu = 0.25$, $\nu' = 0.15$ and $a/|b| = 1$. The nearly isotropic case is shown for comparison. For dip angles different from 0 or 90°, the tensile region is no longer symmetric with respect to the valley's vertical axial plane and extends farther on the left wall of the valley than on the right.
- For a given valley geometry and a given value of the dip angle ψ, the extent of the tensile region depends on the value of the elastic properties. This is shown in Fig. 20 for valleys in a rock mass with horizontal planes of transverse isotropy ($\psi = 0°$), $\nu = 0.25$, $\nu' = 0.15$ and $a/|b| = 1$. The ratios E/E' and G/G' are

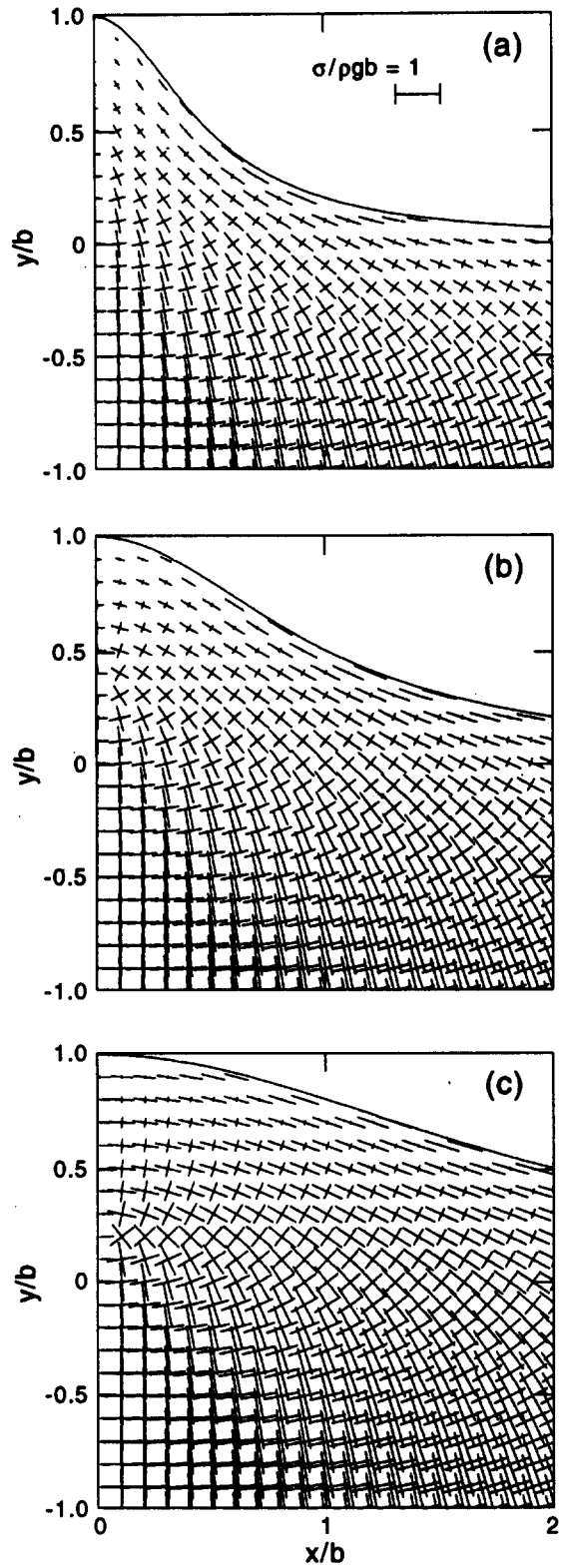

Fig. 14. Principal stress trajectories in transversely isotropic ridges with $a/|b|$ equal to 0.5, 1 or 2 in (a)–(c), respectively. Rock mass with horizontal planes of transverse isotropy and $E/E' = G/G' = 3$, $\nu = 0.25$, and $\nu' = 0.15$.

1 or 3. For a fixed value of G/G', the size of the tensile region decreases as E/E' increases. It also decreases as G/G' increases for a fixed value of E/E'. The extent of the tensile region is very sensitive to the value of the Poisson's ratio ν'. For instance it was found that for a valley in a rock mass with horizontal planes of transverse isotropy with $E/E' = 3$, $G/G' = 1$, $\nu = 0.25$ and $a/|b| = 1$, the size of the tensile region decreases significantly as ν' increases from 0.15 to 0.25 and vanishes for $\nu' = 0.35$.

- For given values of the rock elastic properties and the dip angle of the planes of transverse isotropy, the extent of the tensile region decreases as the topography ratio $a/|b|$ decreases, that is as the valley becomes narrower. An example is shown in Figs 17(a)–(c).

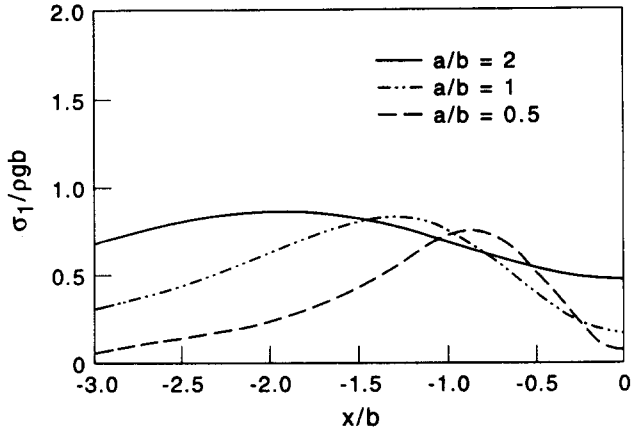

Fig. 15. Variation of the stress ratio $\sigma_1/\rho g|b|$ along the ground surface for the three ridges in Figs 14(a)–(c).

CONCLUSIONS

The analytical method proposed by Pan and Amadei [17] can be used to predict gravitational stresses in long isolated ridges and valleys deforming under a condition of generalized plane strain, e.g. all planes normal to the ridge or valley axis are assumed to warp identically. The method applies to ridges and valleys in generally anisotropic, orthotropic, transversely isotropic and near isotropic rock masses. The magnitude of the predicted stresses is of the order of the characteristic stress $\rho g|b|$ where ρ is the rock density, g is the gravitational

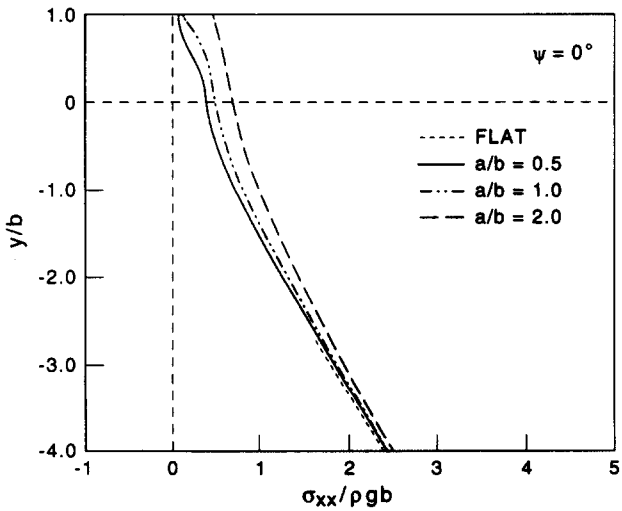

Fig. 16. Variation of the horizontal stress $\sigma_{xx}/\rho g|b|$ with $y/|b|$ along the centerline of the ridges in Figs 14(a)–(c). The short dashed line represents the variation of the standard horizontal stress $\sigma_{xx}/\rho g|b|$ in the absence of topography for this case of anisotropy [4].

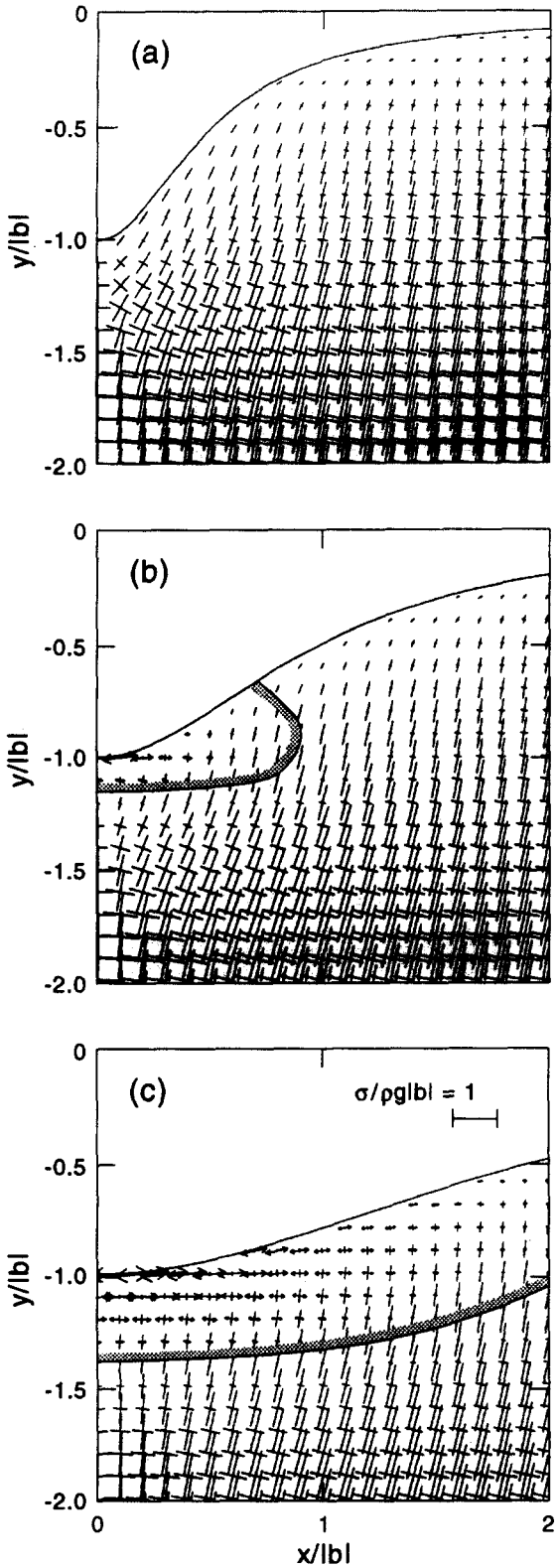

Fig. 17. Principal stress trajectories in transversely isotropic valleys with $a/|b|$ equal to 0.5, 1 or 2 in (a)–(c), respectively. Rock with horizontal planes of transverse isotropy and $E/E' = G/G' = 3$, $\nu = 0.25$ and $\nu' = 0.15$. The shaded regions in (b) and (c) represent the extent of the tensile region at the valley bottom.

acceleration and $|b|$ is the height of the ridge or depth of the valley.

The magnitude and distribution of gravitational stresses in ridges and valleys depend on (1) the ridge and valley geometry defined by the topography ratio $a/|b|$,

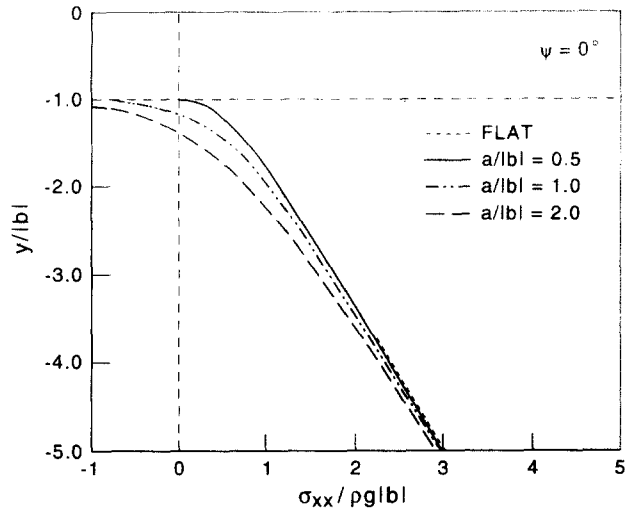

Fig. 18. Variation of the horizontal stress $\sigma_{xx}/\rho g|b|$ with $y/|b|$ along the centerline of the valleys in Figs 17(a)–(c). The short dashed line represents the variation of the standard horizontal stress $\sigma_{xx}/\rho g|b|$ in the absence of topography for this case of anisotropy [4].

(2) the orientation of the anisotropy with respect to the ridge and valley axis (defined by the strike and dip angles of the planes of rock anisotropy) and (3) the degree of rock anisotropy (defined by ratios of elastic constants such as E/E', G/G', ν and ν' for transversely isotropic rocks). At each point in generally anisotropic, orthotropic and transversely isotropic rock masses where the planes of anisotropy are inclined with respect to a ridge or valley axis, the stress field is three-dimensional and the principal stresses are inclined with respect to the plane normal to the ridge or valley axis. For rock masses with planes of transverse isotropy parallel to or normal to a valley or ridge axis, two of the three principal stresses are in the plane normal to that axis and the third principal stress is parallel to that axis.

In the examples presented in this paper, it is shown that when the ground surface is not horizontal the principal stresses are no longer horizontal or vertical.

Table 1. Values of $R_{xx} = (\sigma_{xx} - \sigma_{xxo})/\sigma_{xxo}$ (in percent) at $y/|b| = -4.0$ and $x/|b| = 0$ for ridges and valleys in a nearly isotropic (NI) rock mass and a strongly anisotropic rock mass with $E/E' = G/G' = 3$, $\nu = 0.25$, $\nu' = 0.15$ and $\psi = 0$, 45 and 90°. $a/|b| = 0.5$, 1 and 2

	Ridges			Valleys		
ψ	$a/\|b\| = 2$	$a/\|b\| = 1$	$a/\|b\| = 0.5$	$a/\|b\| = 2$	$a/\|b\| = 1$	$a/\|b\| = 0.5$
0	5.0	1.7	0.8	−6.7	−2.5	−1.3
45	5.2	2.1	1.0	−7.2	−3.1	−1.5
90	10.0	5.0	2.5	−12.5	−5.0	−2.5
NI	7.4	2.9	1.0	−11.5	−4.4	−1.5

Table 2. Values of $R_{xx} = (\sigma_{xx} - \sigma_{xxo})/\sigma_{xxo}$ (in percent) at $y/|b| = -4.0$ and $x/|b| = 3$ for ridges and valleys in a nearly isotropic (NI) rock mass and a strongly anisotropic rock mass with $E/E' = G/G' = 3$, $\nu = 0.25$, $\nu' = 0.15$ and $\psi = 0$, 45 and 90°. $a/|b| = 0.5$, 1 and 2

	Ridges			Valleys		
ψ	$a/\|b\| = 2$	$a/\|b\| = 1$	$a/\|b\| = 0.5$	$a/\|b\| = 2$	$a/\|b\| = 1$	$a/\|b\| = 0.5$
0	6.7	3.3	2.5	−9.2	−5.2	−2.5
45	8.2	5.2	3.1	−12.7	−8.3	−4.9
90	12.5	7.5	5.0	−14.4	−8.7	−6.3
NI	10.4	6.2	3.7	−16.1	−9.3	−5.2

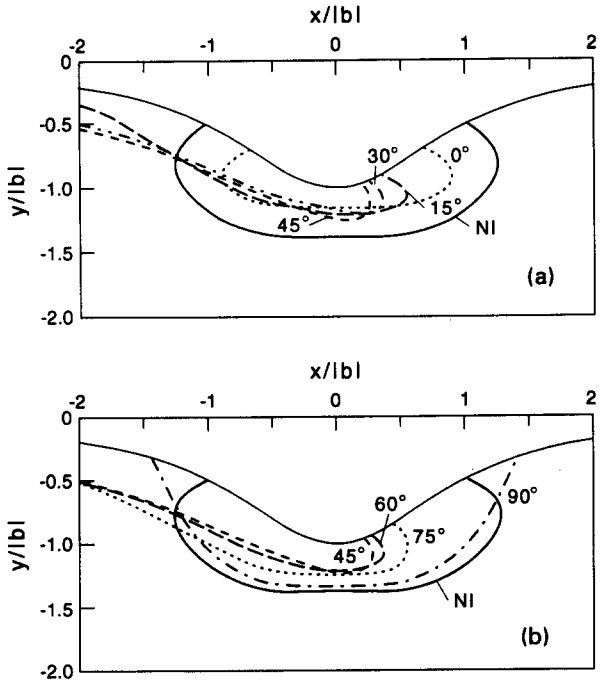

Fig. 19. Extent of the tensile region for values of the dip angle ψ ranging between 0 and 45° in (a) and between 45 and 90° in (b). $E/E' = G/G' = 3$, $\nu = 0.25$, $\nu' = 0.15$ and $a/|b| = 1$. The nearly isotropic case (NI) is also shown for comparison.

Instead, the principal stresses at the ground surface are parallel and perpendicular to the topography (in the absence of surface loads), gradually turning to become horizontal and vertical with depth. The topographic induced stresses become, with increasing depth, asymptotic to the stresses when the ground surface is horizontal. It is found that broader ridges and valleys affect the stress field to a greater depth and to a wider area. These results are the same as those shown by Savage *et al.* [11] for the isotropic case.

As in the isotropic case [11], compression is found to take place in ridge crests and tension in valley bottoms and valley walls. For ridges, the maximum compressive stress is reached on the sides of the ridges. For valleys, the maximum tensile stress is at the valley bottom for horizontal ($\psi = 0°$) and vertical ($\psi = 90°$) planes of anisotropy and on the left wall of the valleys for values of the dip angle ψ between 0 and 90°.

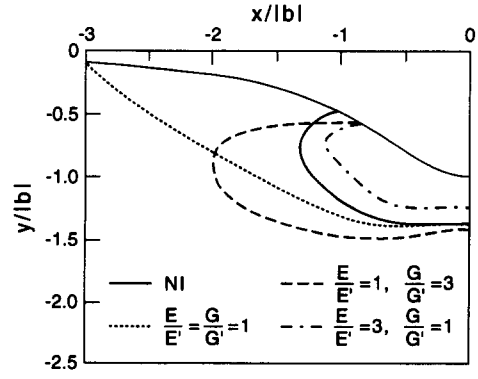

Fig. 20. Extent of the tensile region for horizontal transverse isotropy with E/E' and G/G' equal to 1 or 3. $\nu = 0.25$, $\nu' = 0.15$ and $a/|b| = 1$. The nearly isotropic case (NI) is also shown for comparison.

The method of Pan and Amadei [17] helps to overcome the small slope topography limitation associated with the perturbation method and the isotropic limitation associated with the exact conformal mapping methods. Although the examples presented in this paper are for symmetric ridges or valleys, the method of Pan and Amadei [17] can also be used for asymmetric and more general topographies. The combined effect of gravitational and surface loadings can also be addressed.

Acknowledgement—This research is funded by National Science Foundation, Grant No. MS-9215397.

Accepted for publication 25 October 1993.

REFERENCES

1. Amadei B., Savage W. Z. and Swolfs H. S. Gravitational stresses in anisotropic rock masses. *Int. J. Rock Mech. Min. Sci. & Geomech. Abstr.* **24,** 5–14 (1987).
2. Amadei B., Savage W. Z. and Swolfs H. S. Gravity-induced stresses in stratified rock masses. *Rock Mech. Rock Engng* **21,** 1–20 (1988).
3. Amadei B. and Savage W. Z. Gravitational stresses in regularly jointed rock masses. A keynote lecture. *Proc. Int. Symp. on Fundamentals of Rock Joints*, pp. 463–473, Centek Publ. (1985).
4. Amadei B. and Pan E. Gravitational stresses in anisotropic rock masses with inclined strata. *Int. J. Rock Mech. Min. Sci. & Geomech. Abstr.* **29,** 225–236 (1992).
5. Dolezalova M. Geostatic stress state in cross-anisotropic soil deposits. *Proc. 4th. Danube–European Conference on Soil Mechanics and Foundation Engineering*, Bled, Yugoslavia, pp. 155–160 (1974).
6. Martna J. and Hansen L. Initial rock stresses around the Viestas headrace tunnels no. 2 and 3, Sweden. *Proc. Int. Symp. on Rock Stress and Stress Measurements*, pp. 605–613 (1986).
7. Martna J. Distribution of tectonic stresses in mountainous areas. *Proc. Int. Symp. on Tunneling for Water Resources and Power Projects*, New Delhi (1988).
8. Akhpatelov D. M. and Ter-Martirosyan Z. G. The stressed state of ponderable semi-infinite domains. *Armenian Acad. Sci. Mech. Bull.* **24,** 33–40 (1971).
9. Ter-Martirosyan Z. G., Akhpatelov D. M. and Manvelyan R. G. The stressed state of rock masses in a field body forces. *Proc. 3rd ISRM Congress*, Denver, Part A, pp. 569–574 (1974).
10. Ter-Martirosyan Z. G. and Akhpatelov D. M. The stressed state of an infinite slope with a curvilinear boundary subject to a field of gravity and percolation. *J. Probl. Geomech.* **5,** 81–91 (1972).
11. Savage W. Z., Swolfs H. S. and Powers P. S. Gravitational stress in long symmetric ridges and valleys. *Int. J. Rock. Mech. Min. Sci. & Geomech. Abstr.* **22,** 291–302 (1985).
12. Savage W. Z. and Swolfs H. S. Tectonic and gravitational stress in long symmetric ridges and valleys. *J. Geophys. Res.* **91,** 3677–3685 (1986).
13. McTigue D. F. and Mei C. C. Gravity induced stresses near topography of small slopes. *J. Geophys. Res.* **86,** 9268–9278 (1981).
14. McTigue D. F. and Mei C. C. Gravity induced stresses near axisymmetric topography of small slopes. *Int. J. Num. Analyt. Methods Geomech.* **11,** 257–268 (1987).
15. Liu L. and Zoback M. D. The effect of topography on the state of stress in the crust: Application to the site of the Cajon Pass Scientific Drilling Project. *J. Geophys. Res.* **97,** 5095–5108 (1992).
16. Liao J. J., Savage W. Z. and Amadei B. Gravitational stresses in anisotropic ridges and valleys with small slopes. *J. Geophys. Res.* **97,** 3325–3336 (1992).
17. Pan E. and Amadei B. Stresses in an anisotropic rock mass with irregular topography, *ASCE J. Engng Mech.* **120,** 97–119 (1994).
18. Lekhnitskii S. G. *Theory of Elasticity of an Anisotropic Elastic Body*. Holden-Day, San Francisco (1963).
19. Trummer M. R. An efficient implementation of a conformal mapping method based on the Szegö kernel. *SIAM J. Numer. Anal.* **23,** 853–872 (1986).
20. Muskhelishvili N. I. *Singular Integral Equations*. Noordhoff, Groningen, The Netherlands (1972).

21. Sarkar T. K., Yang X. and Arvas E. A limited survey of various conjugate gradient methods for solving complex matrix equations arising in electromagnetic wave interactions. *Wave Motion* **10**, 527–546 (1988).
22. Muskhelishvili N. I. *Some Basic Problems of the Mathematical Theory of Elasticity*. Noordhoff, Groningen, The Netherlands (1953).
23. Lempriere B. M. Poisson's ratios in orthotropic materials. *J. Am. Inst. Aeronaut. Astronaut.* **6**, 2226–2227 (1968).

APPENDIX

Coefficients b_{ij} and functions $f_i(t)$ in equations (19)–(21):

$$
\begin{aligned}
b_{11} &= (\overline{\mu_2}-\mu_1)(\overline{\lambda_2\lambda_3}-1)-(\overline{\mu_2-\mu_3})\overline{\lambda_3}(\overline{\lambda_2}-\lambda_1)\\
b_{12} &= (\overline{\mu_2}-\mu_2)(\overline{\lambda_2\lambda_3}-1)-(\overline{\mu_2-\mu_3})\overline{\lambda_3}(\overline{\lambda_2}-\lambda_2)\\
b_{13} &= (\overline{\mu_2}-\mu_3)\lambda_3(\overline{\lambda_2\lambda_3}-1)-(\overline{\mu_2-\mu_3})\overline{\lambda_3}(\overline{\lambda_2}\lambda_3-1)\\
b_{21} &= (\overline{\lambda_1\lambda_3}-1)(\overline{\mu_1}-\mu_2)-(\overline{\lambda_1}-\lambda_2)\overline{\lambda_3}(\overline{\mu_1-\mu_3})\\
b_{22} &= (\overline{\lambda_1\lambda_3}-1)(\overline{\mu_1}-\mu_1)-(\overline{\lambda_1}-\lambda_1)\overline{\lambda_3}(\overline{\mu_1-\mu_3})\\
b_{23} &= (\overline{\lambda_1\lambda_3}-1)\lambda_3(\overline{\mu_1}-\mu_3)-(\overline{\lambda_1}\lambda_3-1)\overline{\lambda_3}(\overline{\mu_1-\mu_3})\\
b_{31} &= (\overline{\lambda_1-\lambda_2})\lambda_3(\overline{\mu_1}-\mu_3)-(\overline{\lambda_1}\lambda_3-1)(\overline{\mu_1-\mu_2})\\
b_{32} &= (\overline{\lambda_1-\lambda_2})(\overline{\mu_1}-\mu_1)-(\overline{\lambda_1}-\lambda_1)(\overline{\mu_1-\mu_2})\\
b_{33} &= (\overline{\lambda_1-\lambda_2})(\overline{\mu_1}-\mu_2)-(\overline{\lambda_1}-\lambda_2)(\overline{\mu_1-\mu_2})
\end{aligned}
\tag{A1}
$$

$$
\begin{aligned}
f_1(t) &= [\overline{\mu_2}(\overline{\lambda_2\lambda_3}-1)-(\overline{\mu_2-\mu_3})\overline{\lambda_2\lambda_3}]u(t)\\
&\quad+(\overline{\lambda_2\lambda_3}-1)v(t)-(\overline{\mu_2-\mu_3})\overline{\lambda_3}w(t)\\
f_2(t) &= [\overline{\mu_1}(\overline{\lambda_1\lambda_3}-1)-(\overline{\mu_1-\mu_3})\overline{\lambda_1\lambda_3}]u(t)\\
&\quad+(\overline{\lambda_1\lambda_3}-1)v(t)-(\overline{\mu_1-\mu_3})\overline{\lambda_3}w(t)\\
f_3(t) &= [\overline{\mu_1}(\overline{\lambda_1-\lambda_2})-\overline{\lambda_1}(\overline{\mu_1-\mu_2})]u(t)\\
&\quad+(\overline{\lambda_1-\lambda_2})v(t)-(\overline{\mu_1-\mu_2})w(t)
\end{aligned}
\tag{A2}
$$

where

$$
\begin{aligned}
u(t) &= -\rho g y(t)x'(t)\\
v(t) &= c_1\rho g y(t)y'(t)\\
w(t) &= c_2\rho g y(t)y'(t).
\end{aligned}
$$

If there is a plane of symmetry normal to the z axis, equations (A1) and (A2) reduce to

$$
\begin{aligned}
&b_{11}=\mu_1-\overline{\mu_2},\quad b_{12}=\mu_2-\overline{\mu_2},\quad b_{13}=0\\
&b_{21}=\mu_2-\overline{\mu_1},\quad b_{22}=\mu_1-\overline{\mu_1},\quad b_{23}=0\\
&b_{31}=\overline{\mu_1-\mu_2},\quad b_{32}=0,\quad b_{33}=0
\end{aligned}
\tag{A3}
$$

and

$$
\begin{aligned}
f_1(t) &= -\overline{\mu_2}u(t)-v(t)\\
f_2(t) &= -\overline{\mu_1}u(t)-v(t)\\
f_3(t) &= -(\overline{\mu_1-\mu_2})w(t)=0.
\end{aligned}
\tag{A4}
$$